

Airfoil Table Generation and Validation for the VR-12 and SSC-A09 Airfoils and Quadrotor Performance Prediction

<p>Kristen Kallstrom Aerospace Engineer NASA Ames Research Center Moffett Field, CA, USA</p>	<p>Dorsa Shirazi Aerospace Engineer NASA Ames Research Center Moffett Field, CA, USA</p>
---	---

ABSTRACT

As part of NASA’s Urban Air Mobility (UAM) mission, the Revolutionary Vertical Lift Technology (RVLT) project is creating rotorcraft reference designs that can be used by the rotorcraft community to develop quiet, efficient, and safer air vehicles. At NASA, this effort is made possible by the use of the RVLT toolchain software. Airfoil tables are often a critical part of the conceptual design process as they inform both comprehensive analysis and Computational Fluid Dynamics (CFD) codes of 2D aerodynamic coefficients, such as lift, drag, and moment coefficients. These airfoil tables, typically generated during experimental testing, are often proprietary and thus not widely distributable; further, there is not always clear or available reference documentation that provides information on the test conditions. The airfoil tables from these experiments are referred to in this work as Legacy airfoil tables. The scope of this study is to generate airfoil tables with the NASA OVERset grid CFD FLOW solver (OVERFLOW) coupled with the AirFoil Table Generator (AFTGen) software and validate these airfoil tables based on performance predictions calculated in Comprehensive Hierarchical Aeromechanics Rotorcraft Model (CHARM). The overall goal is to provide CFD generated airfoil tables, validate them through comprehensive analysis, and publish the airfoil tables for public distribution. The RVLT quadrotor reference model was selected as the basis for all analyses. The quadrotor uses the VR-12 and SSC-A09 airfoils for its rotor blades. Simulations were run in OVERFLOW for the VR-12 and SSC-A09 airfoils for $\pm 20^\circ$ angles of attack, Mach numbers from 0.3 to 1.0, and a Reynolds-Mach proportionality constant of 1.023×10^7 . The C81 format airfoil tables from AFTGen were then blended with Legacy NACA 0012 airfoil table data for $\pm 20^\circ$ to $\pm 180^\circ$ angle of attack range. CHARM was used to compute thrust coefficient, power coefficient, and figure of merit for an isolated rotor in hover using proprietary legacy airfoil tables for the VR-12 and SSC-A09, as well as with the OVERFLOW generated airfoil tables for the VR-12 and SSC-A09. Overall, the OVERFLOW and Legacy performance predictions agreed well, with the best correlation between simulated and Legacy data observed with the VR-12 airfoil tables.

NOTATION

<p>c chord length (ft) c_d section drag coefficient $c_{d,min}$ minimum drag coefficient c_l section lift coefficient $c_{l,max}$ maximum lift coefficient c_m section moment coefficient C_P power coefficient, $P/\rho A(\Omega R)^3$ C_P/σ ratio of power coefficient to solidity C_T thrust coefficient, $T/\rho A(\Omega R)^2$ C_T/σ ratio of thrust coefficient to solidity FM figure of merit M Mach number M_{DD} drag divergence Mach number</p>	<p>M_{tip} tip Mach number r radial location (ft) R blade radius (ft) Re Reynolds number Re/M Reynolds-Mach proportionality constant t/c maximum thickness-to-chord ratio V_∞ free stream velocity x/c chord location, from leading edge, normalized by chord α angle of attack (deg) η number of normal grid points θ blade twist angle (deg) μ advance ratio ξ number of periodic grid points σ rotor solidity, thrust-weighted Ω angular velocity (rad/s)</p>
--	---

Presented at the Vertical Flight Society’s 6th Decennial Aero-mechanics Specialists’ Conference, Santa Clara, CA, Feb. 6-8, 2024. This paper is declared a work of the U.S. Government and is not subject to copyright protection in the United States.

INTRODUCTION

NASA’s Urban Air Mobility (UAM) mission is driven by the need to research and develop quieter, more efficient, and safer vertical take-off and landing (VTOL) vehicles. UAM concept vehicles can be used to focus and guide NASA research activities in support of VTOL and electric VTOL (eVTOL) air taxi development. NASA’s Revolutionary Vertical Lift Technology (RVLT) project supports this effort through the implementation of toolchain software programs that encourage and facilitate government and industry efforts to meet UAM needs. The UAM reference models were developed within the RVLT mission to provide valuable simulations and experimental research for public use to benefit the rotorcraft community [1–7]. Figure 1 provides an overview of some of the NASA RVLT reference models.

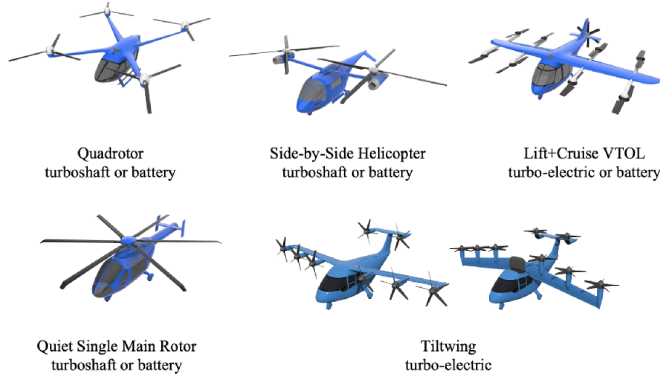


Figure 1. RVLT reference models [2, 4–6, 8].

The quadrotor reference model has a number of variants that meet a range of missions [4]. These reference vehicles are sized and analyzed for one, four, and six occupants for both electric and turboshaft propulsion. Table 1 contains the characteristics of the six-occupant turboshaft and electric quadrotor models. Details of the rotor and blade properties are included in Table 2.

The design, sizing, and analysis of the reference vehicles is accomplished using the RVLT toolchain software programs, such as the NASA Design and Analysis of Rotorcraft (NDARC) [9, 10], Comprehensive Analytical Model of Rotorcraft Aerodynamics and Dynamics (CAMRAD II) [11–13], and the Comprehensive Hierarchical Aeromechanics Rotorcraft Model (CHARM) [14, 15]. For aerodynamic design and performance analysis of edgewise rotors, airfoils (and airfoil tables) representative of current technology are required. For the RVLT reference vehicles, the airfoils used are the VR-12 (inboard of 0.85R) and SSC-A09 (at the tip). The airfoil names and radial stations were provided from existing comprehensive analysis models being used in the iterative design process for the quadrotor reference vehicle. The VR-12 and SSC-A09 radial stations (r/R), twist (θ), chord length (c), and maximum thickness-to-chord ratio (t/c) are shown in Table 3.

Table 1. Quadrotor reference vehicle characteristics for the six-occupant configurations [1, 2].

Characteristic	Units	Turboshaft	Electric
payload	lb	1,200	1,200
rotor radius	ft	9.1	13.8
disk loading	lb ft ²	3.5	3.0
tip speed	ft/s	450	450
power	hp	2x294	4x181
DGW	lb	3,678	7,221
empty weight	lb	2,282	6,012
structure	lb	1,033	1,853

Table 2. Quadrotor’s rotor parameters for 6-occupant turboshaft model [1, 2].

Parameter	Units	Value
airfoils	-	SSC-A09 VR-12
number of rotors	-	4
number of blades	-	3
blade radius	ft	9.10
rotor disk area, A_{disk}	ft ²	263.60
chord, c	ft	1.44
tip speed	ft/s	550
linear twist	deg	-12
linear taper	-	0.75

Table 3. Quadrotor geometry.

r/R	θ [deg]	c [ft]	t/c	Airfoil
0.00	9.0	0.685	0.109	VR-12
0.12	7.5	0.685	0.109	VR-12
0.25	6.0	0.545	0.109	VR-12
0.50	3.0	0.406	0.109	VR-12
0.85	-1.2	0.211	0.109	VR-12
0.95	-2.4	0.155	0.090	SSC-A09
1.00	-3.0	0.514	0.090	SSC-A09

Airfoil Tables

Often when running comprehensive analysis and CFD simulations, the Legacy airfoil tables provide 2D aerodynamic performance data from experimental tests that may differ from desired flight conditions. Further, there is often not much detailed information on how these tables were generated. To complicate the use of these Legacy tables, the experimental test data utilized in their generation is often proprietary and cannot be publicly distributed. For this reason, there is interest in investigating the capability of CFD programs, such as OVERFLOW, to match these Legacy datasets. Good comparison between OVERFLOW calculated airfoil tables and experimental Legacy airfoil tables could enable the rotorcraft community to more confidently generate airfoil tables to meet design, sizing, and analysis needs.

The Legacy airfoil tables for the VR-12 and SSC-A09, referenced throughout this work, were generated by Boeing and

Sikorsky during experimental testing for the RAH-66 Comanche helicopter. Although not much information is known about the specifics of these experiments, a number of papers have been published over the years investigating the performance capability of these modern rotorcraft airfoils.

The Boeing Vertol (VR) series airfoils, including the VR-7/8, and VR-12/15 airfoils, were tested in the Boeing Vertol V/STOL Wind Tunnels, during which Mach-scaled isolated rotor tests were completed for various blade planforms [16]. Model data from this test campaign was then used to estimate the full-scale rotor performance for each configuration tested [17]. The VR-12 airfoil was also the focus of studies analyzing airfoil performance with and without modifications such as a leading edge slat [18, 19], variable droop leading edge [20], and miniature trailing edge effectors [21].

In 1984, Flemming performed a study of the SSC-A09, SSC-A07, SSC-B08, SC1095, and SC1094R8 airfoils in NASA’s Eleven-Foot Transonic Wind Tunnel [22]. The airfoils were tested at Mach numbers ranging from Mach 0.3 to 1.07, stagnation pressures from 1.0 to 1.4 atm, and static temperatures of approximately 530° R (70° F). The wind tunnel test campaign was a joint NASA and Sikorsky effort to analyze different SSC airfoils and compare them with the drag divergence Mach number for the original SC series airfoils. Data from this report is used for benchmark comparisons against OVERFLOW simulations for the SSC-A09 airfoil.

APPROACH

The airfoil tables for the quadrotor reference vehicle were generated using AFTGen, a program developed by Sukra-Helitek, Inc. [23]. AFTGen provides a graphic user interface (GUI) interface for flow solvers such as XFOIL [24], MSES [25], ARC2D [26], UNS2D [27], and OVERFLOW [28]. OVERFLOW is a high-order, structured, Reynolds-averaged Navier-Stokes (RANS) flow solver developed by Nichols and Buning that is currently used by NASA and industry alike. OVERFLOW was coupled with AFTGen to calculate the section lift, drag, and moment coefficients of the SSC-A09 and VR-12 airfoils. The OVERFLOW solver incorporates laminar, turbulent, and transition flow models. Simulations were run assuming fully turbulent flow and completing using the Spalart-Allmaras turbulence model [29, 30]. The number of trailing edge points used was set to 33 total points at the trailing edge, using methodology discussed in Reference 31. The stretching ratio, which governs the distance between the periodic points of the grid, was set to 1.1. The grid layer spacing in the normal direction was defined using three parameters: the extrusion layer spacing mode was set to hyperbolic tangent, the domain radius was 50 chords, and the y^+ value was set to 1.0. A steady state switching to time accurate algorithm was used in simulations, which allows the solver to switch to time accurate integration if the steady state solution begins to diverge.

The airfoil coordinate files were obtained from the University of Illinois at Urbana-Champaign (UIUC) airfoil database [32].

The coordinate points from $0 \leq x/c \leq 0.15$ around the leading edge were entered into a script to increase the point density using cubic spline interpolation. Increasing the number of leading edge points smooths out the geometry and improves AFTGen’s built-in gridding capability, as discussed by Kallstrom [31]. Figure 2 shows the airfoil profiles for the VR-12 and SSC-A09 airfoils as generated in AFTGen.

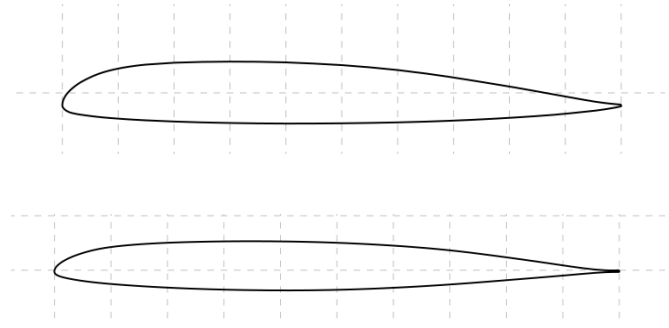


Figure 2. VR-12 (top) SSC-A09 (bottom) airfoil profiles.

AFTGen with OVERFLOW

A grid resolution study was performed to determine a grid that results in a 1% or less change between grid sizes. First, the total number of periodic points (grid points along the airfoil surface in the wraparound direction, ξ) was swept from 201 to 801 grid points. The normal points (the number of grid points from the surface outward to the grid boundary, η) were held fixed at a coarse 101 points during this first sweep. Once the periodic points converged to a value of less than 1%, the periodic points were then fixed, and the normal points were swept from 101 to 801 until a percent change of 1% or less was achieved. A simple example of an O-grid is provided in Figure 3.

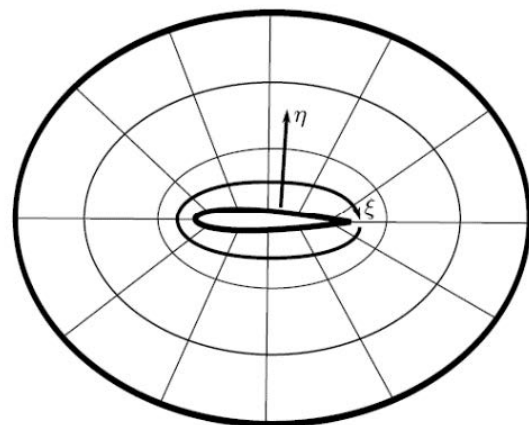


Figure 3. OVERFLOW O-grid generated in AFTGen.

The results showed that 501 periodic and 401 normal points were sufficient for the SSC-A09 airfoil, while the VR-12 airfoil required 601 periodic and 501 normal points to reach the same convergence criteria. To minimize computation time, cases were run at standard atmospheric flow conditions. The Reynolds/Mach proportionality constant (Re/M) reflects these

conditions, the chord length, and the expected flight speeds. The Mach number (M) for each airfoil is selected based on the Mach number range available on its respective Legacy airfoil table. The angle of attack (α) range for the table encompasses $\pm 20^\circ$. For values exceeding $\pm 20^\circ$, the standard NACA 0012 airfoil table data was used to populate α - M pairs up to $\pm 180^\circ$ α [33, 34]. Table 4 contains the atmospheric conditions, Re/M , Mach number range, α range, and grid size used in the simulations run on the Pleiades supercomputer.

Table 4. AFTGen inputs for SSC-A09 and VR-12 airfoil table generation.

	Units	SSC-A09	VR-12
ρ	slug/ft ³	0.002377	0.002377
T	K	294	294
Re/M	-	1.023×10^7	1.023×10^7
μ	slug.s/ft	3.737×10^{-7}	3.737×10^{-7}
ξ	-	501	601
η	-	401	501
α	deg	± 20	± 20
M	-	0.30, 0.40, 0.50, 0.60, 0.70, 0.80, 0.85, 0.92, 0.98	0.310, 0.355, 0.406, 0.454, 0.502, 0.550, 0.600, 0.650, 0.701, 0.750, 0.802, 0.824, 0.852, 1.000

AIRFOIL TABLE RESULTS

The airfoil tables for the VR-12 and SSC-A09 airfoil sections were completed using the Pleiades supercomputer at NASA Ames Research Center and the settings specified in Table 4. Cases were divided into low Mach number runs at Mach 0.3, mid-range Mach numbers from 0.4 to 0.7, and transonic to sonic Mach numbers from 0.8 to 1.0. Mach numbers less than 0.3 are not shown in this study to avoid the need for low-Mach preconditioning. Time per case ranged from 5 hours to as many as seven days for high angle of attack and Mach number pairs. For unconverged cases, the specific α -Mach pair was rerun when possible, and linearly interpolated otherwise. The converged results from 0 to $\pm 20^\circ$ were then compared with the existing Legacy airfoil tables for Mach numbers from 0.3 to 1.0. The average delta in the aerodynamic coefficients, maximum lift versus Mach number, and minimum drag coefficient versus Mach number are presented.

VR-12

The OVERFLOW generated airfoil table for the VR-12 resulted in a reasonable comparison with the Legacy aerodynamic coefficients for lower angle of attack values. From -5° to 10° , the correlation between simulated and experimental data was good. However, there was some discrepancy between the predicted maximum lift coefficients at each Mach number.

In general, the OVERFLOW calculation for the maximum lift coefficient was less than the Legacy value, although the trends

are similar. Further, into the post stall region, there was not consistency between the lift curves for the Legacy and OVERFLOW data. The maximum lift at Mach numbers from 0.3 to 0.5 has reasonable agreement, although OVERFLOW calculates a lower value than shown in Legacy data. Beyond Mach 0.5, there is a noticeable drop in maximum lift for OVERFLOW calculations when compared with the Legacy data. The maximum lift coefficient versus Mach number is plotted in Figure 4. This figure contains a fourth order best fit polynomial for each data set to smooth out results. The delta between the simulated and experimental maximum lift coefficient is shown in Figure 5.

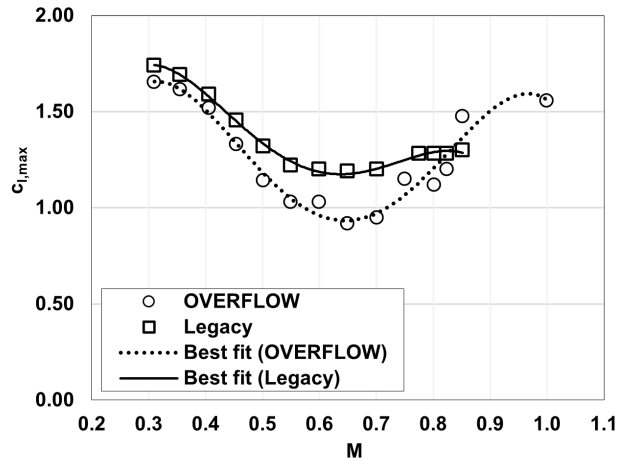


Figure 4. Maximum lift coefficient versus Mach number for the VR-12 airfoil.

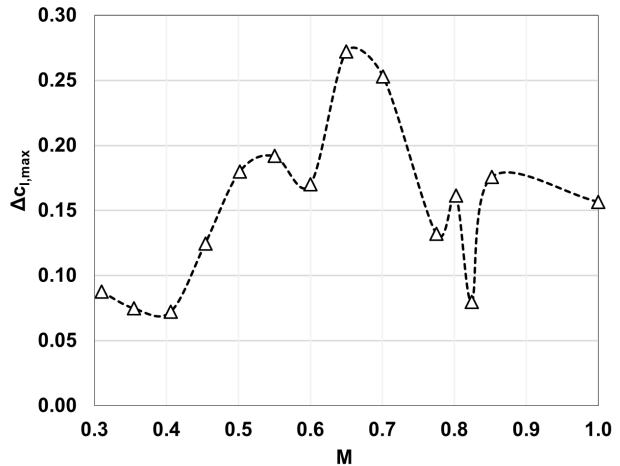


Figure 5. Change in maximum lift coefficient versus Mach number for the VR-12 airfoil.

The discrepancy in the calculation for the maximum lift coefficient could be explained by the chord length, and thus, the Reynolds number, used to generate the airfoil table. For both the SSC-A09 and VR-12 airfoil tables, it was mentioned previously that the conditions used to generate the airfoil tables were obtained from Flemming's SSC-A09 data report, as there was no specific reference for the source of the Legacy

VR-12 airfoil table [22]. The large delta in the OVERFLOW and Legacy results is likely a result of a different chord length used in the experimental data set. The Re/M , calculated using this chord length, would similarly differ from the experimental data included in the Legacy airfoil table.

In contrast, the agreement between the minimum drag coefficient for the Legacy and OVERFLOW airfoil tables is good. For each Mach number, the simulated and experimental minimum drag coefficient matches well, with the minimum drag increasing once the Mach number approaches the transonic range. In Figure 6, the minimum drag coefficient versus Mach number is plotted for both the OVERFLOW and Legacy airfoil tables. The average delta between the simulated and experimental results is shown in Figure 7. There is a clear increase in both drag and lift around Mach 0.8, indicating that the drag divergence Mach number, M_{DD} , occurs around this value. It should be noted that the minimum drag coefficient delta comparison between Legacy and OVERFLOW data is non-zero, although it is very small.

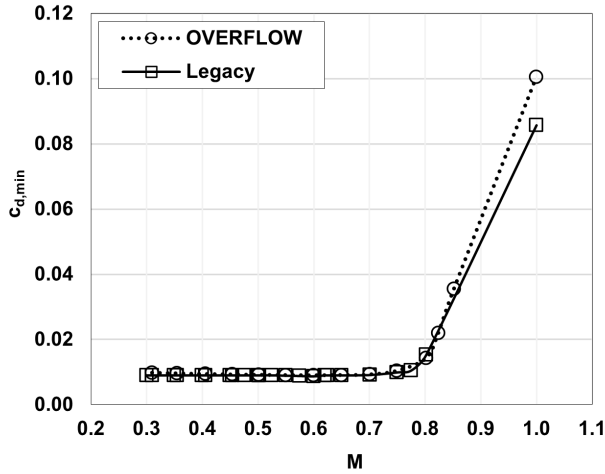


Figure 6. Minimum drag coefficient versus Mach number for the VR-12 airfoil.

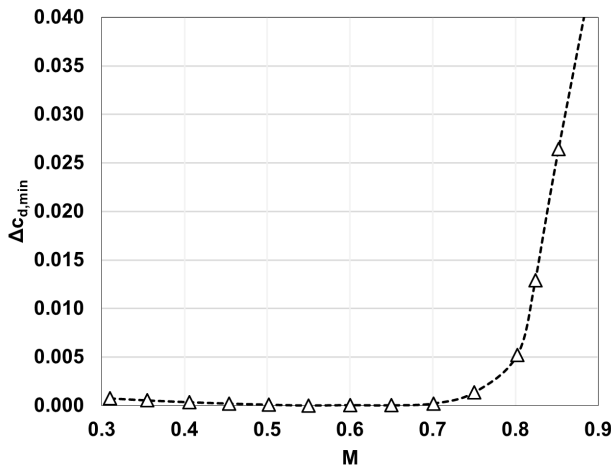


Figure 7. Change in minimum coefficient versus Mach number for the VR-12 airfoil.

A table of the maximum lift coefficient and minimum coefficient delta at each Mach number is included in Appendix A, Table 5. The average delta for the lift, drag, and moment coefficients at each Mach number in the OVERFLOW and Legacy airfoil tables is similarly included in Appendix A, Table 6.

SSC-A09

The OVERFLOW generated SSC-A09 airfoil table shows reasonable agreement with the Legacy data; however, there is an overall discrepancy between the Legacy and OVERFLOW aerodynamic coefficients. The discrepancy with the SSC-A09 simulated results is typically in the form of a higher predicted lift coefficient than seen in Legacy results from angles of attack from approximately -5° to 5° , particularly at Mach numbers from 0 to 0.3 and beyond Mach 0.8. The simulated and experimental maximum lift coefficient versus Mach number, as well as the change in maximum lift coefficient versus Mach number, are shown in Figures 8 and 9.

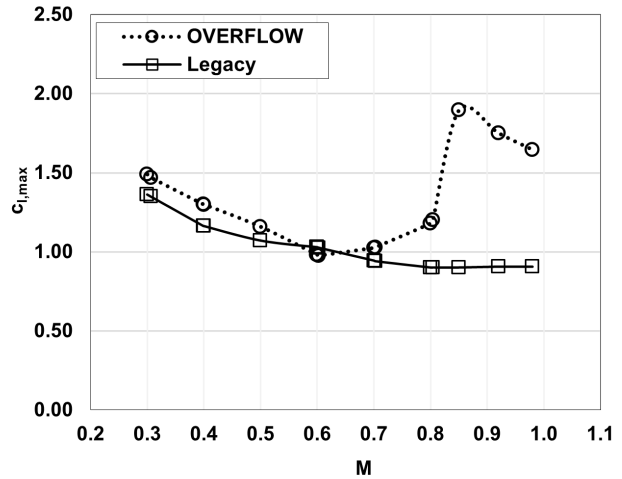


Figure 8. Maximum lift coefficient versus Mach number for the SSC-A09 airfoil.

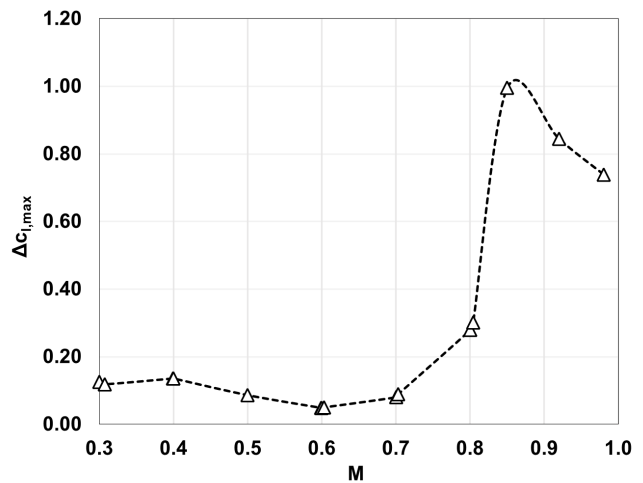


Figure 9. Change in maximum lift coefficient versus Mach number for the SSC-A09 airfoil.

With respect to the maximum lift coefficient versus Mach number shown in Figure 8, the OVERFLOW results show a slightly higher maximum lift calculation than present in the Legacy data from Mach 0.3 to 0.5, with the closest similarity seen at Mach 0.6. At Mach 0.7, there is a slight increase in lift for the OVERFLOW calculation, followed by a sharp increase in lift at Mach 0.8 and 0.85. Around these Mach numbers, the Mach drag divergence Mach number occurs. This drag divergence Mach number, which occurs around Mach 0.8, is indicated by an increase in both lift and drag aerodynamic coefficients. The simulated and experimental minimum drag coefficient versus Mach number, as well as the change in minimum drag coefficient versus Mach number, are shown in Figures 10 and 11. Figures 10 and 11 show a generally good agreement between the minimum drag coefficient calculated by OVERFLOW and the Legacy data; particularly good agreement is shown from Mach numbers 0.3 through 0.8. Around Mach 0.85, the drag begins to increase, with the OVERFLOW drag values significantly greater than those in the Legacy results.

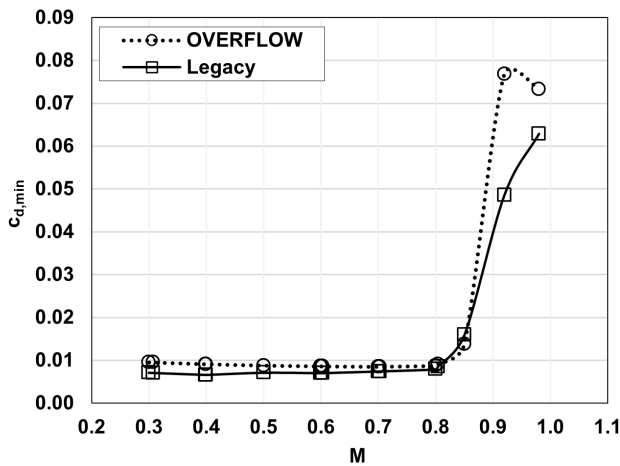


Figure 10. Minimum drag coefficient versus Mach number for the SSC-A09 airfoil.

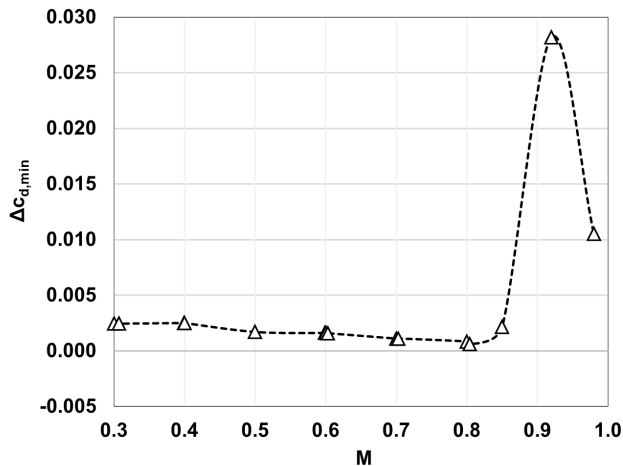


Figure 11. Change in minimum drag coefficient versus Mach number for the SSC-A09 airfoil.

The delta values for the minimum drag coefficient and maximum lift coefficient are tabulated in Table 7, which is included in Appendix A. The average delta for the lift, drag, and moment coefficients at each Mach number in the OVERFLOW and Legacy airfoil tables is similarly included in Appendix A, Table 8.

As expected from comparisons with the Legacy data, the OVERFLOW results did show reasonable agreement with the experimental results, with some discrepancies observed when the curves approach the maximum lift coefficient and stall regions for the airfoil. As an additional check for the OVERFLOW airfoil table, a drag polar comparison for the OVERFLOW data and available data published by Flemming was completed.

Figures 12, 13, 14, 15, 16, and 17 compare the experimental and simulated datasets for Mach numbers ranging from 0.307 to 0.804. The Legacy data, while not shown in these figures, agreed quite well with the experimental data.

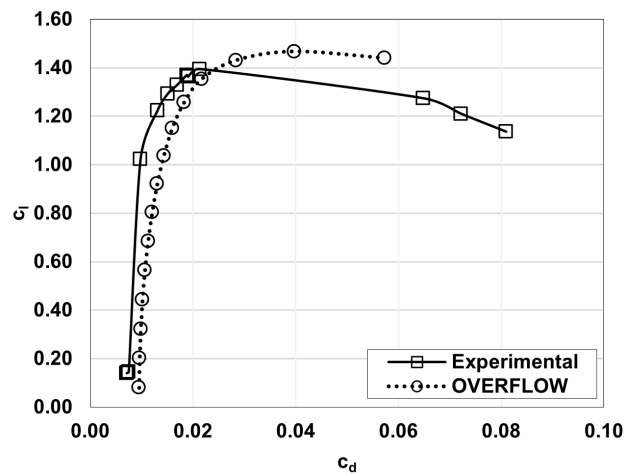


Figure 12. OVERFLOW vs Flemming drag polar for the SSC-A09 airfoil at Mach 0.307.

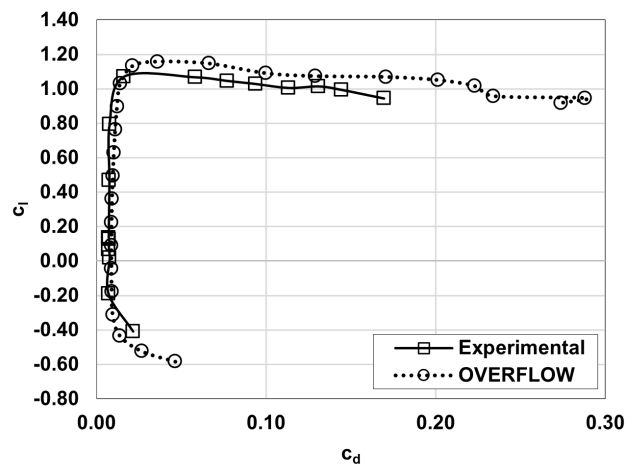


Figure 13. OVERFLOW vs Flemming drag polar for the SSC-A09 airfoil at Mach 0.5.

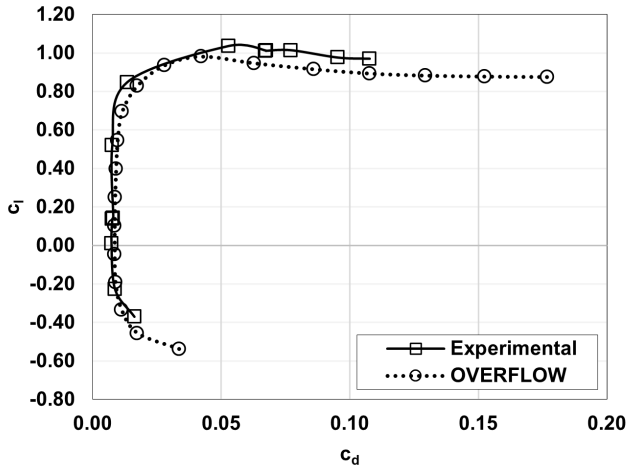


Figure 14. OVERFLOW vs Flemming drag polar for the SSC-A09 airfoil at Mach 0.599.

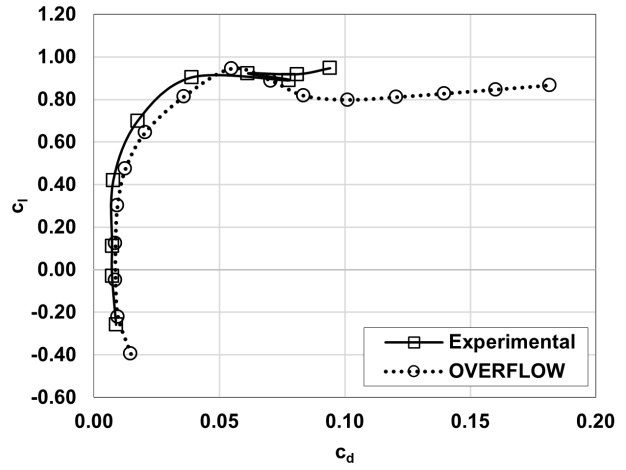


Figure 16. OVERFLOW vs Flemming drag polar for the SSC-A09 airfoil at Mach 0.703.

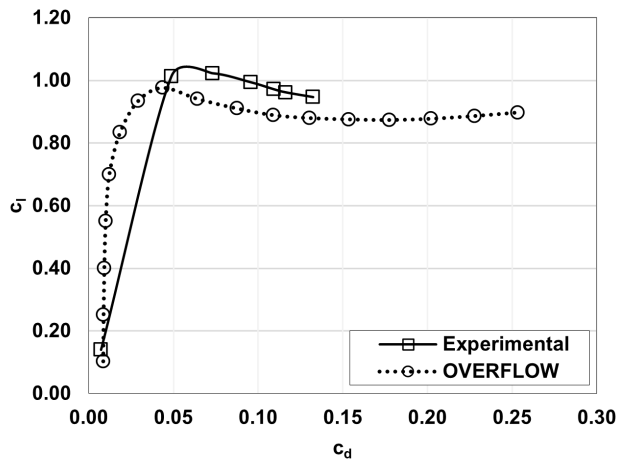


Figure 15. OVERFLOW vs Flemming drag polar for the SSC-A09 airfoil at Mach 0.603.

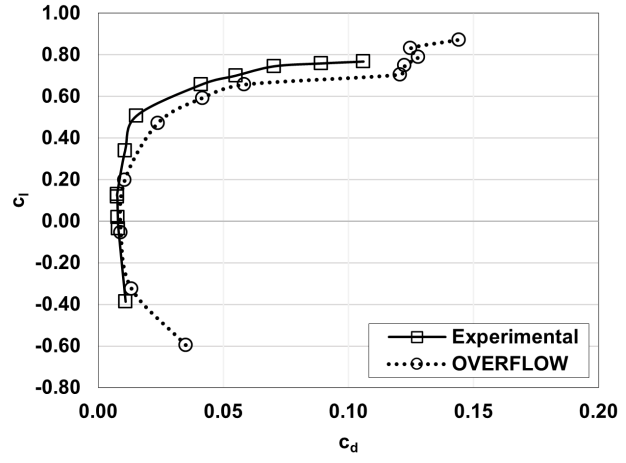


Figure 17. OVERFLOW vs Flemming drag polar for the SSC-A09 airfoil at Mach 0.804.

Potential Sources of Error

Although the agreement between the OVERFLOW generated airfoil tables and Legacy airfoil tables is generally good, there are some potential sources of error that should be considered.

1. Actual testing conditions and the Reynolds number for these airfoil tables is not presently well documented. The airfoil tables were generated using a chord-based Reynolds number and atmospheric conditions reported by Flemming in Reference 22, thus, the exact conditions of the airfoil tables were not matched.
2. A comprehensive understanding of the test setup and conditions is imperative for precisely comparing 2D simulations with experimental data. This is not always possible when using Legacy airfoil tables in which the test setup and conditions are not available, documented, and/or proprietary.

3. Aerodynamic phenomena at stall and post-stall conditions may impact OVERFLOW's capability to precisely match experimental test conditions. The turbulence model used in simulations could potentially influence simulated results, and could be explored further to investigate if other turbulence models may provide more accurate results when compared with Legacy experimental data. Smith explores the effect of turbulence models in CFD calculations in Reference 35. Shelton similarly explores turbulence model modifications and the effect those modifications have on how well simulated and experimental data correlate in Reference 36.
4. As the Mach number increased, particularly past Mach 0.6, the discrepancy between the Legacy and OVERFLOW tables also increased. It's possible that some portions of the airfoil are experiencing transonic flow, which suggests the presence of shock waves that could potentially result in simulation inaccuracies. This should be investigated in future work to visualize and verify this phenomenon as a factor in simulation accuracy.

5. There may be some potential errors in experimental tests that could influence the correlation between CFD calculations and the test data. These errors can't reasonably be quantified, due to unknowns with respect to the test conditions themselves.
6. Any corrections made to the Legacy airfoil tables were similarly, at present, not documented, which could influence the comparison between the OVERFLOW simulations and the Legacy airfoil tables.

COMPREHENSIVE ANALYTICAL TOOLS

CHARM is a comprehensive VTOL aircraft analysis code developed by Continuum Dynamics Inc. (CDI). The CHARM software is capable of modeling VTOL aircraft aerodynamics in maneuvering and steady flight conditions. CHARM allows the user to define flow and body characteristics, including the rotor geometry, aerodynamic conditions, wind tunnel speed, and airfoil tables as input files. CHARM models the aircraft aerodynamic and dynamic interactions using a combination of Fast Vortex/Fast Panel Solution methods [37–42]. Its objective is to provide reasonably accurate results for aerodynamic interactions with short computational time when compared with a higher-fidelity CFD solver. The quadrotor airfoil tables generated in AFTGen with OVERFLOW and the Legacy airfoil tables were formatted into airfoil table input files for CHARM. These input files are used as a reference in comprehensive analysis simulations to provide the aerodynamic coefficients experienced at each radial station.

CHARM RESULTS

To better examine the quality of each newly generated airfoil table, each OVERFLOW airfoil table was compared to the respective Legacy airfoil table. CHARM was utilized to simulate a single isolated three-bladed rotor with a 9.10-ft radius in free field, a linear twist of -12° and a linear taper of 0.75, and a cutout at 12.09% of the rotor radius. Simulations were completed at RPMs of 350, 400, 469, and 500 ($M_{tip} = 0.276 - 0.395$) and a collective sweep from 0° to 11° . The coefficient of thrust (C_T), coefficient of power (C_P), and figure of merit (FM) values for the OVERFLOW tables versus the Legacy airfoil results were then compared.

The CHARM analysis was split into three cases. Case 1 defines the radial stations along the blade span solely with the VR-12 airfoil and airfoil tables. In case 1, simulations were run once with VR-12 Legacy airfoil table and once with VR-12 OVERFLOW airfoil table. Case 2 repeats the process with the radial stations along the blade span instead fully defined by the SSC-A09 airfoil and airfoil tables. Similarly, case 2 simulations were run separately for the SSC-A09 Legacy airfoil table and with the SSC-A09 OVERFLOW airfoil table. In case 3, the radial stations are defined by the VR-12 airfoil spanning from the blade root to 85% of the blade radius and SSC-A09 airfoil from 0.95R to the tip of the rotor blade. Table 3 illustrates the geometry of the quadrotor and the airfoil radial locations on the rotor span.

Case 1: Single Rotor in Hover - VR-12 airfoil

A single isolated rotor was simulated with the quadrotor blade geometry in CHARM and utilized the VR-12 airfoil table for the entire span of the blade. Two sets were simulated: a set using the Legacy airfoil table and another with the OVERFLOW airfoil table. Each CHARM case was completed for a collective sweep from 0° to 13° .

Figures 18, 19, 20, and 21 show FM versus C_T/σ at RPM values of 350, 400, 469, and 500 ($M_{tip} = 0.276 - 0.395$). Each data point presented in these figures is the result of an average of over 100 rotor revolutions.

The VR-12 case results indicate that the OVERFLOW airfoil table set predicts a lower FM than the Legacy airfoil table. These results indicate that at RPMs of 469 and 500, the peak FM that can be achieved is at approximately $0.75 C_T/\sigma$, while the RPM 350 and 400 reach the FM peak at a higher C_T/σ value. The OVERFLOW prediction for VR-12 airfoil table experiences its peak FM at a lower C_T/σ value sooner than the Legacy prediction. For both the OVERFLOW and Legacy data set, the last data point occurs at a collective of 13° . It is evident that at this collective, a higher C_T/σ was predicted for the Legacy airfoil table. The Legacy data set for VR-12 shows the FM peak as high as 0.8, which is a less realistic FM value than the peak FM of approximately 0.75 shown with the OVERFLOW airfoil table.

Figures 22, 23, 24, and 25 present C_P/σ versus C_T/σ for a collective sweep from 3° to 13° in 2° increments at RPMs of 350, 400, 469, and 500. The results indicate that the OVERFLOW is predicting higher C_P/σ values at C_T/σ values greater than 0.08. Also, the Legacy airfoil table set has a higher prediction for C_T/σ at all collective angles and for all RPMs. As RPM increases, the Legacy and OVERFLOW results have a closer prediction value for C_P/σ . Also, at RPMs of 469 and 500, the C_T/σ has a closer prediction of $\sim \Delta C_T/\sigma = 0.0043$ compared to smaller RPM of 350 and 400 ($\sim \Delta C_T/\sigma = 0.0068$).

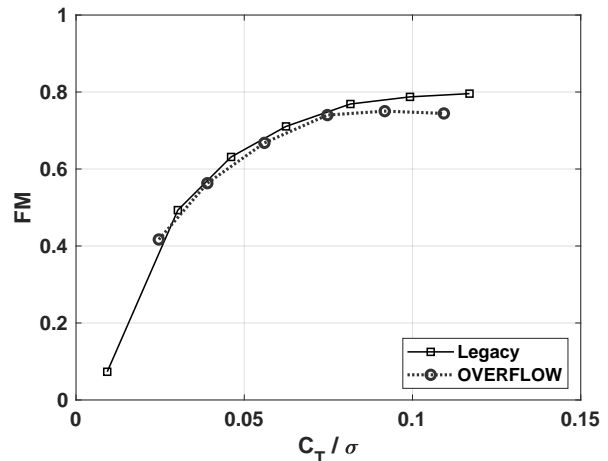


Figure 18. Single isolated rotor at 350 RPM, VR-12 airfoil tables ($M_{tip}=0.276$).

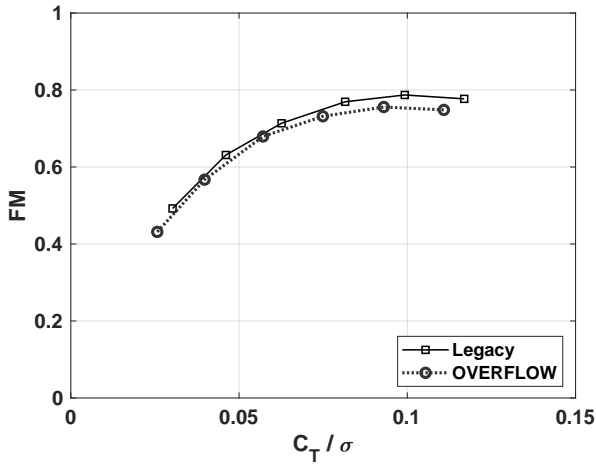


Figure 19. Single isolated rotor at 400 RPM, VR-12 airfoil tables ($M_{tip}=0.316$).

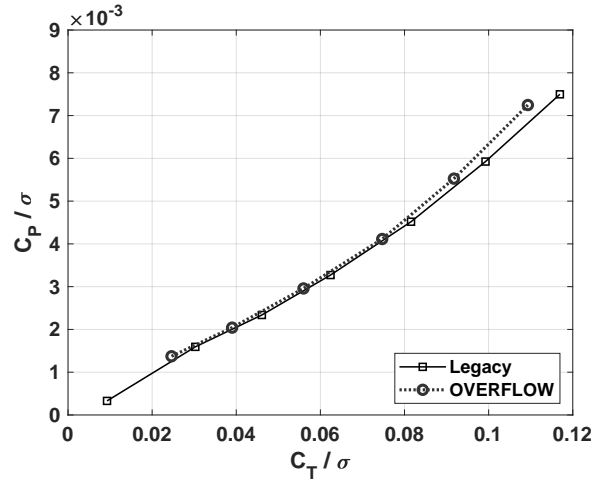


Figure 22. VR-12 airfoil table for single isolated rotor at 350 RPM ($M_{tip}=0.276$).

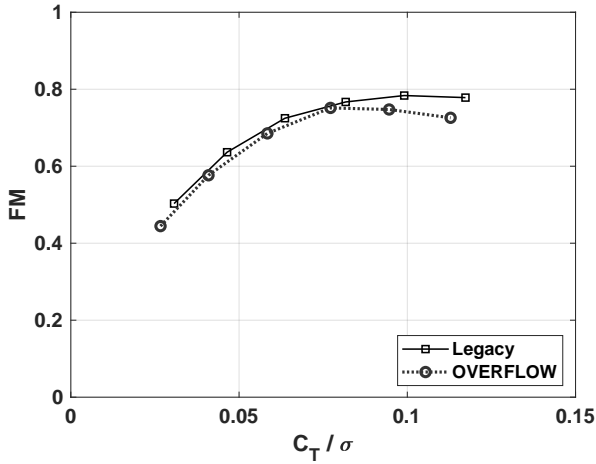


Figure 20. VR-12 airfoil table for single isolated rotor at 469 RPM ($M_{tip}=0.370$).

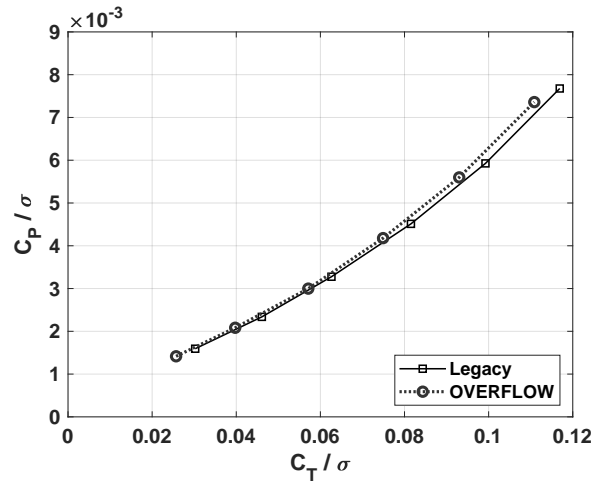


Figure 23. VR-12 airfoil table for single isolated rotor at 400 RPM ($M_{tip}=0.316$).

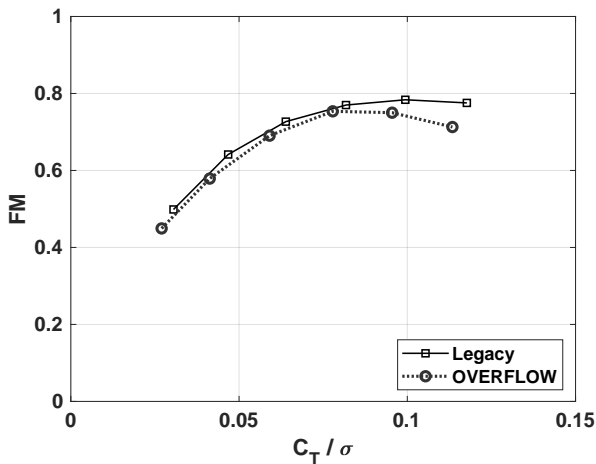


Figure 21. VR-12 airfoil table for single isolated rotor at 500 RPM ($M_{tip}=0.395$).

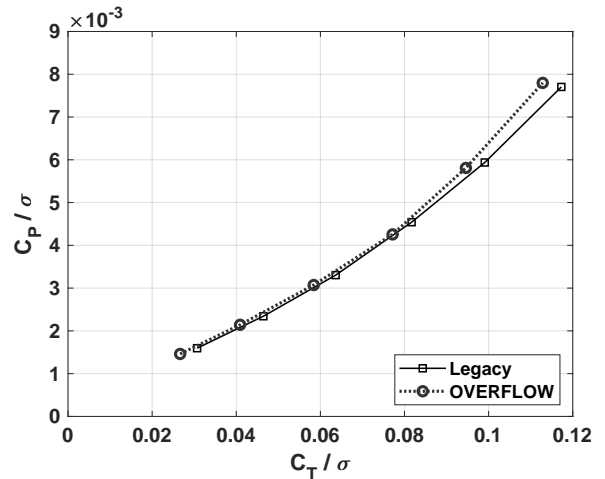


Figure 24. VR-12 airfoil table for single isolated rotor at 469 RPM ($M_{tip}=0.370$).

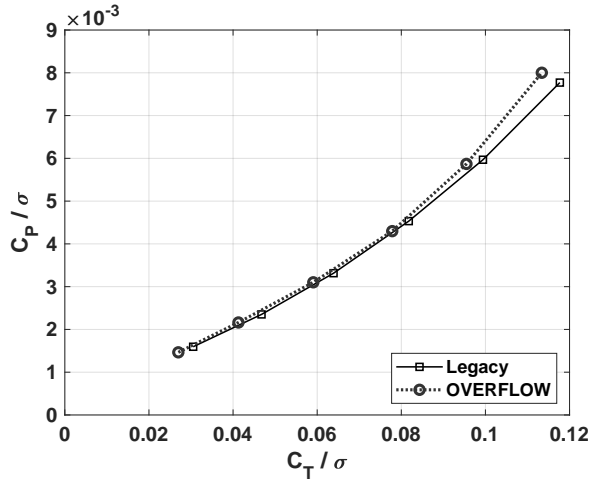


Figure 25. VR-12 airfoil table for single isolated rotor at 500 RPM ($M_{tip}=0.395$).

To better compare the power and thrust predictions of each airfoil table, the C_T/σ versus collective angle and C_P/σ versus collective were plotted and studied. Additional VR-12 results and figures detailing C_T/σ and C_P/σ versus collective can be found in Appendix B.

Figures 46, 47, 48, and 49 present the C_P/σ versus collective angle for four RPM of 350, 400, 469 and 500. These figures show that the Legacy results for collective angles from 3° to 11° have a higher power prediction than the OVERFLOW results. However, OVERFLOW results for RPMs of 469 and 500 at collective angles between 11° to 13° have higher predicted power values. Overall, the OVERFLOW and Legacy airfoil table at RPMs of 469 and 500 correlated better, with an average $\Delta 0.0004$ between the OVERFLOW and Legacy power predictions. The power prediction difference between the OVERFLOW and Legacy results is lowest at higher RPM and at collective angles of 3° and 13° ($\Delta C_P/\sigma = 0.00013$ and $\Delta C_P/\sigma = -0.00022$).

Figures 42, 43, 44, and 45 show the VR-12 results for C_T/σ versus collective angle for RPMs of 350, 400, 469, and 500. These results indicate that the OVERFLOW airfoil table input results in a lower predicted thrust value at all four RPM values simulated throughout the collective sweep compare to the Legacy airfoil table input. The thrust value prediction difference between OVERFLOW and Legacy cases decreases by ~ 0.002 at the higher RPMs of 469 and 500. Results using the Legacy airfoil table show that C_T/σ values are less sensitive to changes in RPM when compared with results using the OVERFLOW airfoil table.

Case 2: Single Rotor in Hover - SSC-A09 airfoil

The same rotor geometry was used for the SSC-A09 cases as was used for the VR-12 cases, with the SSC-A09 airfoil instead used for the entire rotor span. Cases were completed using the SSC-A09 OVERFLOW airfoil table inputs and repeated using the Legacy airfoil table. As with the VR-12

cases, the CHARM simulations were completed for collective angles from 0° to 13° in increments of 2° , RPM values at 350, 400, 469, and 500, and simulated for an average of over 100 rotor revolutions. The SSC-A09 results for FM versus C_T/σ are shown in Figures 26, 27, 28, and 29. These results indicate that Legacy airfoil table inputs result in a peak FM prediction of 0.81m while the OVERFLOW airfoil table inputs results in a peak FM of 0.77. Both of the FM predictions yield high peak values; however, OVERFLOW's slightly smaller FM prediction is more reasonable.

Figures 30, 31, 32, and 33 show the C_P/σ versus C_T/σ results from cases run with the OVERFLOW and Legacy SSC-A09 airfoil tables. These results indicate at RPMs of 469 and 500, the difference between the power prediction of Legacy and OVERFLOW cases is $\Delta C_P/\sigma = 0.0005$. Also, at lower collective angles, the C_T/σ predictions are closer between Legacy and OVERFLOW. Overall, OVERFLOW has the higher C_P/σ prediction for every RPM simulated. For the same value of C_P/σ , the Legacy results yield a higher prediction of C_T/σ at all RPMs.

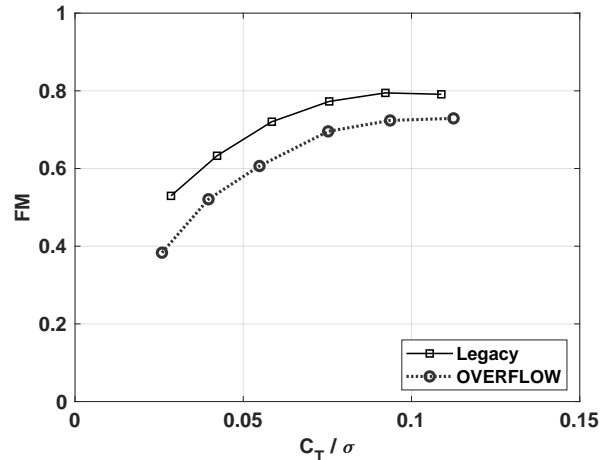


Figure 26. SSC-A09 airfoil table for single isolated rotor at 350 RPM ($M_{tip}=0.276$).

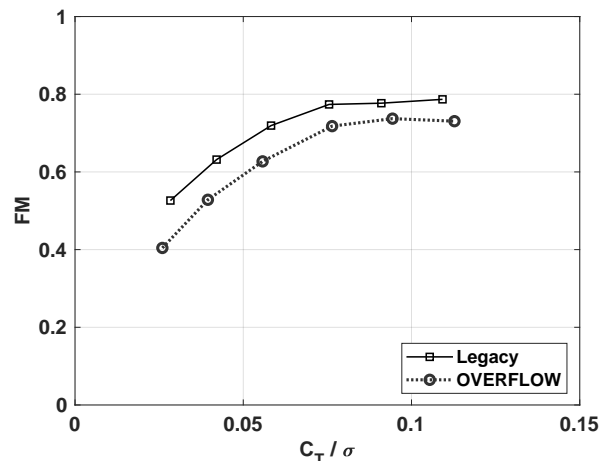


Figure 27. SSC-A09 airfoil table for single isolated rotor at 400 RPM ($M_{tip}=0.316$).

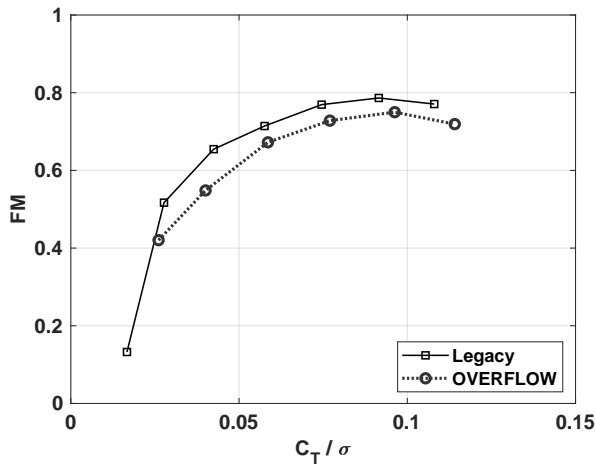


Figure 28. SSC-A09 airfoil table for single isolated rotor at 469 RPM ($M_{tip}=0.370$).

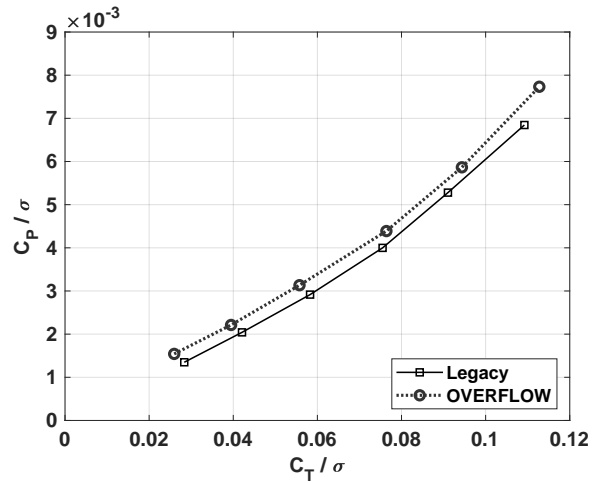


Figure 31. SSC-A09 airfoil table for single isolated rotor at 400 RPM ($M_{tip}=0.316$).

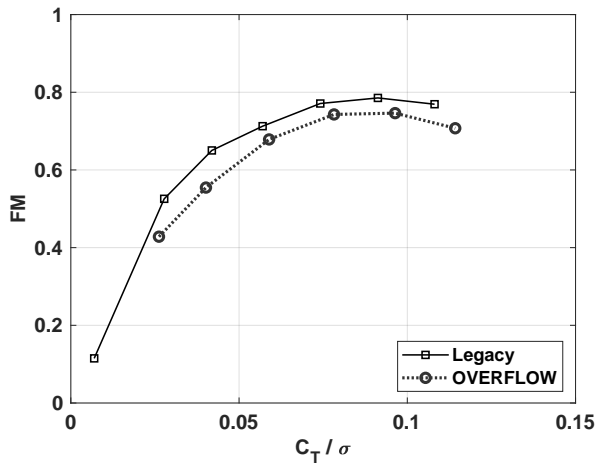


Figure 29. SSC-A09 airfoil table for single isolated rotor at 500 RPM ($M_{tip}=0.395$).

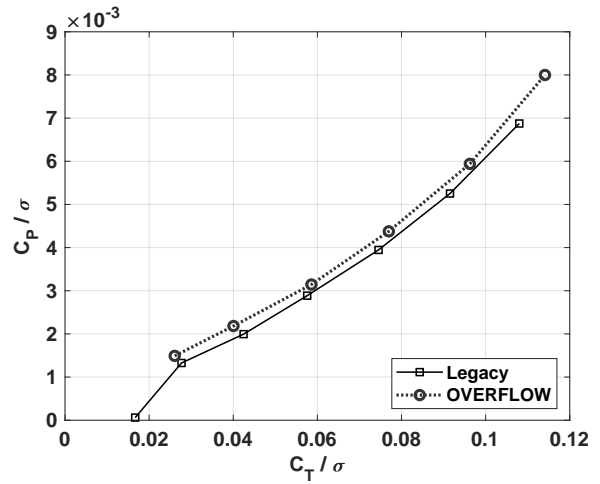


Figure 32. SSC-A09 airfoil table for single isolated rotor at 469 RPM ($M_{tip}=0.370$).

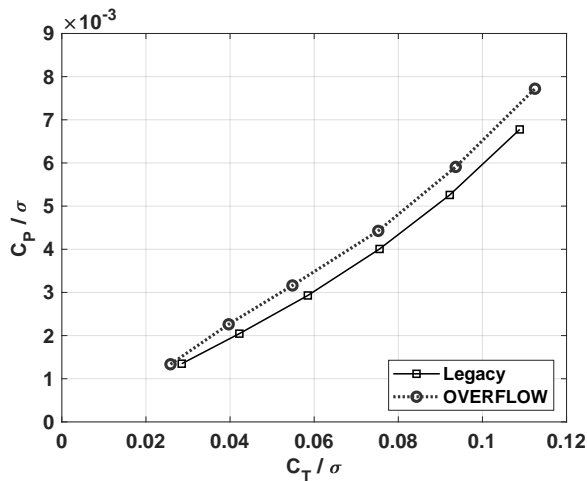


Figure 30. SSC-A09 airfoil table for single isolated rotor at 350 RPM ($M_{tip}=0.276$).

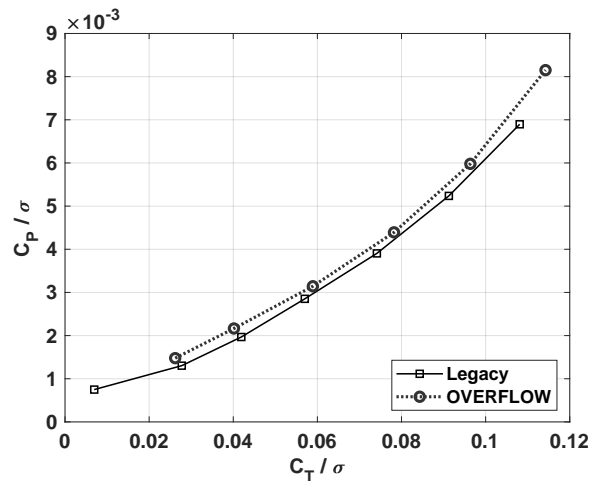


Figure 33. SSC-A09 airfoil table for single isolated rotor at 500 RPM ($M_{tip}=0.395$).

Additional SSC-A09 results and figures detailing C_T/σ and C_P/σ versus collective can be found in Appendix C. Figures 54, 55, 56, and 57 show C_T/σ versus collective. OVERFLOW cases show a higher C_T/σ prediction at collective angles of 9, 11, and 13° and lower C_T/σ prediction for collective angles smaller than 9° at RPMs of 350 and 400, Figures 54 and 55. At RPMs of 450 and 500, and at collective angles exceeding 9°, the OVERFLOW and Legacy C_T/σ predictions have a difference as large as $\Delta C_T/\sigma = 0.0048$ compared to the RPM cases of 350 and 400 that have $\Delta C_T/\sigma = 0.0022$. The OVERFLOW cases have a lower C_T/σ prediction compared to the Legacy cases for collective angles smaller than 9° at RPMs of 350 and 400, and at collective angles smaller than 7° for RPMs of 469 and 500. At RPMs of 469 and 500, and collective angles exceeding 7°, the OVERFLOW results produce a higher C_T/σ prediction than the Legacy results. Figures 58, 59, 60, and 61 show the C_P/σ versus collective angle at four different RPMs. These results indicate that OVERFLOW has a higher C_P/σ prediction for all collective angles; further, as the collective angle increases, the difference between the C_P/σ prediction for Legacy and OVERFLOW cases grows as well. Similarly, as RPM increases, the OVERFLOW C_P/σ prediction increases. In contrast, the Legacy results show a smaller sensitivity of C_P/σ to RPM changes.

Case 3: Quadrotor Single Rotor in Hover - Both Airfoils

The quadrotor single rotor cases include the same rotor blade geometry that was used previously for the individual VR-12 and SSC-A09 cases. However, for the quadrotor single rotor cases, the VR-12 and SSC-A09 airfoil profiles were used to define the whole rotor blade airfoil profile, as shown in Table 3. The VR-12 airfoil table was used starting at the root up to 0.85R and followed by the SSC-A09 airfoil table from the radial station at 0.95 to the tip of the blade. Similar to previous runs, the collective angle sweep of 0, 3, 5, 7, 9, 11, and 13° was done for RPMs of 350, 400, 469, and 500 for both Legacy and OVERFLOW airfoil tables. CHARM cases were simulated for an average of over 100 rotor revolutions. Figures 34, 35, 36, and 37 show FM versus C_T/σ for quadrotor single rotor cases at four different RPMs. As seen previously, the Legacy prediction for FM is higher compared to that of OVERFLOW for all RPMs. Also, the Legacy predictions reach the FM peak at a higher C_T/σ compared to OVERFLOW predictions.

Figures 38, 39, 40, and 41 show C_P/σ versus C_T/σ at 350, 400, 469, and 500 RPM. For each set of Legacy and OVERFLOW data, the last three data points reflect collective angles of 9, 11, and 13°. At a collective angle larger than 9°, the largest difference for $\Delta C_P/\sigma$ and $\Delta C_T/\sigma$ predictions is observed between the OVERFLOW and Legacy results. These results indicate that at the same collective angle, Legacy results have a higher C_T/σ prediction compared to OVERFLOW. Also, the results demonstrate that the Legacy results have less sensitivity to RPM changes than OVERFLOW.

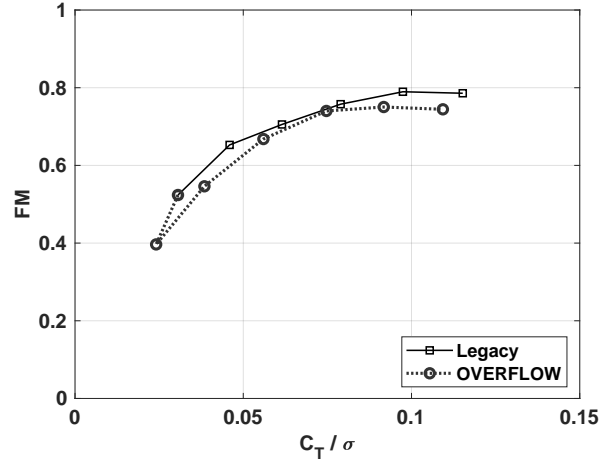


Figure 34. Quadrotor airfoil table for single isolated rotor at 350 RPM ($M_{tip}=0.276$).

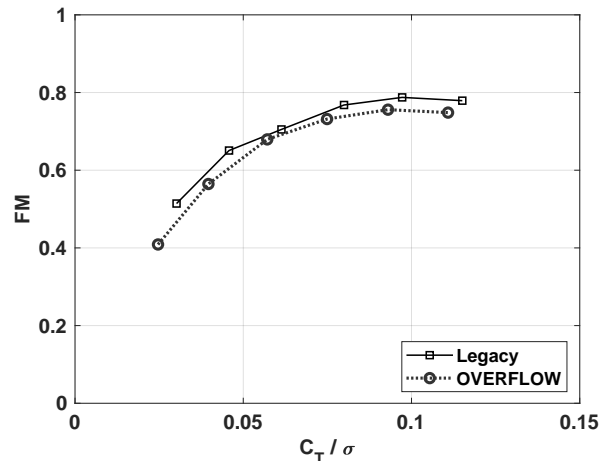


Figure 35. Quadrotor airfoil table for single isolated rotor at 400 RPM ($M_{tip}=0.316$).

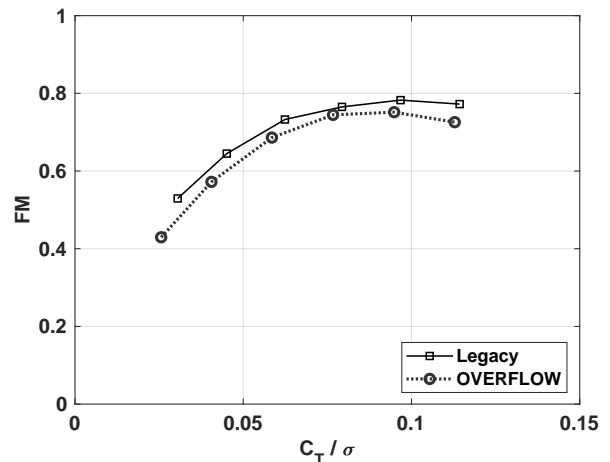


Figure 36. Quadrotor airfoil table for single isolated rotor at 469 RPM ($M_{tip}=0.370$).

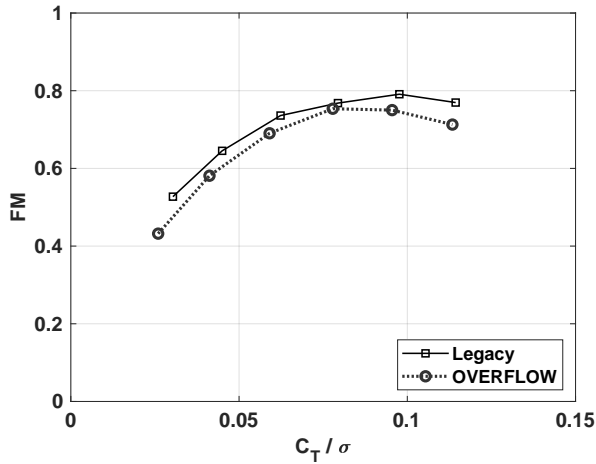


Figure 37. Quadrotor airfoil table for single isolated rotor at 500 RPM ($M_{tip}=0.395$).

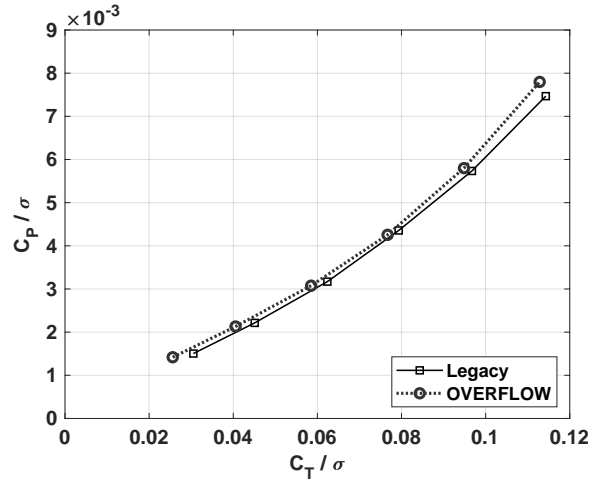


Figure 40. Quadrotor airfoil table for single isolated rotor at 469 RPM ($M_{tip}=0.370$). RPM500

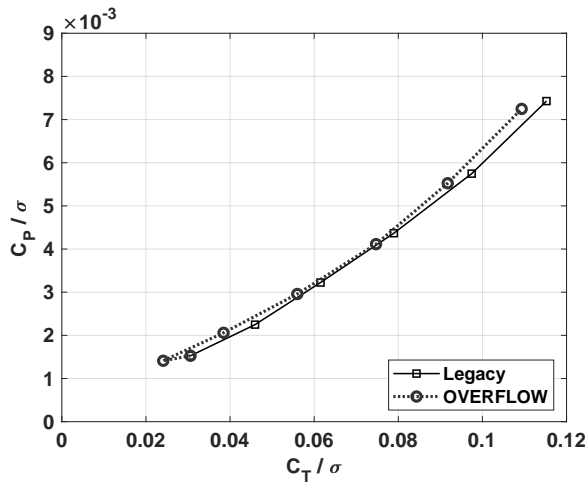


Figure 38. Quadrotor airfoil table for single isolated rotor at 350 RPM ($M_{tip}=0.276$).

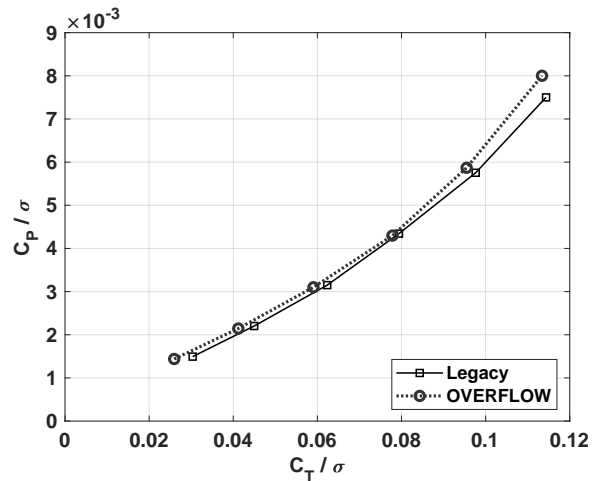


Figure 41. Quadrotor airfoil table for single isolated rotor at 500 RPM ($M_{tip}=0.395$).

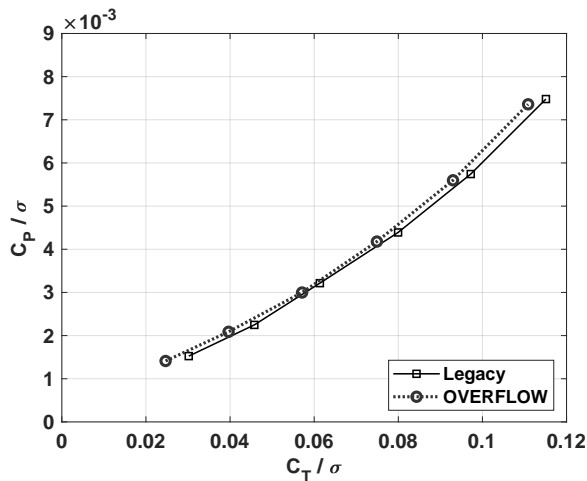


Figure 39. Quadrotor airfoil table for single isolated rotor at 400 RPM ($M_{tip}=0.316$).

Additional quadrotor single rotor results and figures can be found in Appendix D. Figures 66, 67, 68, and 69 show the C_P/σ versus collective angle. OVERFLOW shows a lower C_P/σ prediction at 350 and 400 RPM, but closer agreement has been observed between OVERFLOW and Legacy results for C_P/σ predictions at RPMs of 469 and 500. The results also indicate that at a collective angle smaller than 9° , and at RPMs of 469 and 500, OVERFLOW cases predict a lower C_P/σ compared to the Legacy cases. However, at collective angles greater than 9° , the OVERFLOW cases predict higher C_P/σ values. Additionally, at RPM values of 469 and 500 and a collective angle of 13° , the difference between Legacy and OVERFLOW cases is as large as $\Delta C_P/\sigma = 0.0005$. Figures 70, 71, 72, and 73 show C_T/σ results for the collective angle sweep. These results show that for all RPM values swept, the Legacy cases predict a greater C_T/σ than the OVERFLOW cases. Also, at RPMs of 469 and 500, the Legacy and OVERFLOW cases show a closer C_T/σ prediction, with

$\Delta C_T/\sigma = 0.0029$. The 350 and 400 RPM cases, comparatively, result in a greater difference between the Legacy and OVERFLOW cases, where $\Delta C_T/\sigma = 0.0053$. These results indicate that OVERFLOW cases require a higher collective angle than Legacy cases to reach the same C_T/σ value.

CONCLUDING REMARKS

Two airfoil tables were generated using AFTGen with OVERFLOW from 0° to $\pm 20^\circ$ and blended with the Legacy NACA 0012 airfoil table for angles of attack exceeding $\pm 20^\circ$ up to $\pm 180^\circ$. Comparisons between the maximum lift coefficients and minimum drag coefficient were completed for the 2D data, with good agreement between OVERFLOW generated airfoil tables and the Legacy airfoil tables. Analyses for the airfoil tables are summarized below.

- Results between the VR-12 OVERFLOW and Legacy airfoil tables shows that OVERFLOW generally predicts a lower $c_{l,max}$ than is seen in the Legacy data. The closest agreement is seen at lower Mach numbers from 0 to 0.45, with the discrepancy in $c_{l,max}$ increasing as the Mach number increases up until Mach 0.8.
- Results between the VR-12 OVERFLOW and Legacy airfoil tables shows that OVERFLOW and Legacy data are in good agreement with respect to $c_{d,min}$, with OVERFLOW results showing an increase in predicted drag from Mach 0.85 until Mach 1.0.
- Results between the SSC-A09 OVERFLOW and Legacy airfoil tables shows that OVERFLOW generally predicts a higher $c_{l,max}$ than is seen in the Legacy data. From Mach 0.3 to 0.6, there is a clear offset between the there is a clear offset between the $c_{l,max}$ values of the two tables; however, the discrepancy in $c_{l,max}$ increases as the Mach number increases, up until Mach 0.8.
- Results between the SSC-A09 OVERFLOW and Legacy airfoil tables shows that OVERFLOW generally predicts a slightly higher $c_{d,min}$ than exists in the Legacy airfoil table. However, the difference in the calculated OVERFLOW $c_{d,min}$ and the Legacy $c_{d,min}$ is quite small, and shows good agreement. From Mach 0.6 to Mach 0.85, the simulated and experimental data sets show a larger difference in minimum section drag.

The OVERFLOW and Legacy airfoil tables were formatted into airfoil table input files for CHARM. These input files were used for free field, isolated rotor hover simulations for three cases. Case 1 represents only the VR-12 airfoil across the entire blade span, case 2 represents only the SSC-A09 airfoil across the entire blade span, and case 3 represents the quadrotor single rotor case. In the quadrotor single rotor case, the VR-12 airfoil spans from the blade root to 0.85%R and the SSC-A09 spans from 0.95%R to the blade tip. The CHARM results can be summarized as follows:

- For the single airfoil profile VR-12 rotor, there is good agreement between cases with the OVERFLOW and Legacy airfoil table input files, with the OVERFLOW cases resulting in a slightly lower peak FM than the Legacy cases for each RPM simulated. On average, over four RPMs of 350, 400, 469, and 500, the $\Delta C_T/\sigma$ is 0.0054 with a minimum of 0.0035 and a max difference of 0.0076. The difference between the power prediction of both sets of airfoil tables also has a good agreement with an average of $\Delta C_P/\sigma = 0.0002$, minimum delta of 0.0001, and maximum of 0.0004.
- For the single airfoil profile SSC-A09 rotor, a good agreement was observed between both sets of airfoil tables. The results show the average difference between the C_T/σ between the Legacy and OVERFLOW is 0.0028 with a minimum of 0.0003 and a maximum $\Delta C_T/\sigma$ of 0.0061. Also, these results indicate the average $\Delta C_P/\sigma$ was 0.0028, with a minimum delta of ~ 0.00 and a maximum delta of 0.0013.
- For the rotor containing both the VR-12 and SSC-A09 airfoil profiles (the quadrotor blade), the results show great agreement for C_P/σ with average $\Delta C_P/\sigma = 0.0001$ and minimum of ~ 0.00 and maximum of 0.0005. Also, the C_T/σ results showed a good agreement between two airfoil tables with $\Delta C_T/\sigma = 0.0041$, minimum difference of 0.0010, and maximum difference of 0.0075.

Overall, the CHARM results indicate that the OVERFLOW and Legacy airfoil tables had better C_T/σ agreement for the VR-12 and better C_P/σ agreement for the SSC-A09. The CHARM results for the OVERFLOW and Legacy cases show small deltas in performance predictions for FM, C_T/σ , and C_P/σ , supporting the publication of the OVERFLOW tables for government and industry use with some considerations to be addressed in future work.

FUTURE WORK

The airfoil tables generated for this work are not currently included in the appendices, as there are still some considerations that need to be addressed prior to their publication.

- The maximum lift coefficient discrepancy between OVERFLOW and Legacy airfoil tables should be investigated, and the potential limitations of OVERFLOW in stall and post-stall conditions, as well as the potential limitations of experimental testing in this region, should be explored.
- The transition between the OVERFLOW airfoil tables and the NACA 0012 airfoil table at $\pm 20^\circ$ and beyond needs to be smoothed out to avoid discontinuities between the two airfoil tables.
- Improvements to the OVERFLOW airfoil tables, as described above, will ultimately be documented in a NASA Technical Memorandum. This same approach could be

applied to other modern rotorcraft airfoils to validate their use in comprehensive analyses for other reference vehicles, and additional OVERFLOW generated airfoil tables could be published for use by the rotorcraft community.

Author Contact Information

Kristen Kallstrom kristen.kallstrom@nasa.gov
Dorsa Shirazi dorsa.shirazi@nasa.gov

ACKNOWLEDGMENTS

The authors would like to acknowledge the mentorship and support of Dr. Wayne Johnson, Dr. Gloria Yamauchi, Chris Silva, and Dr. William Warmbrodt. This work could not have been completed without Ethan Romander, who makes the magic happen on our local Linux computer, Pegasus, and the Pleiades supercomputer. Thank you to Nick Peters, Stephen Wright, and Sesi Kottapalli for reviewing and providing excellent feedback and recommendations. Thank you to Witold Koning and Jason Cornelius for the discussions and suggestions on airfoil table generation, both using AFTGen and OVERFLOW. Thank you to Lauren Weist, and Natasha Schatzman for the discussions and suggestions as this work progressed. Thank you to Jason Lechniak and double thanks to Sesi Kottapalli for the respective quadrotor CHARM and CAMRADII models used as a reference in this work. Thank you to Brian Allan, Joseph Derlaga, and Pieter Buning for providing resources and suggestions for continued exploration of airfoil table generation with OVERFLOW in the future. This work was completed with the support of the Revolutionary Vertical Lift Technology Project.

REFERENCES

1. Johnson, W., Silva, C., and Solis, E., "Concept Vehicles for VTOL Air Taxi Operations," American Helicopter Society Technical Conference on Aeromechanics Design for Transformative Vertical Flight, San Francisco, CA, January 2018.
2. Johnson, W., and Silva, C., "NASA concept vehicles and the engineering of advanced air mobility aircraft," *The Aeronautical Journal*, Vol. 126, (1295), 2022, pp. 59–91. DOI: 10.1017/aer.2021.92.
3. Silva, C., Johnson, W., and Solis, E., "Multidisciplinary Conceptual Design for Reduced-Emission Rotorcraft," American Helicopter Society Technical Conference on Aeromechanics Design for Transformative Vertical Flight, San Francisco, CA, January 2018.
4. Silva, C., Johnson, W., Antcliff, K. R., and Patterson, M. D., "VTOL Urban Air Mobility Concept Vehicles for Technology Development," 2018 Aviation Technology, Integration, and Operations Conference, Atlanta, GA, June 2018. DOI: <https://doi.org/10.2514/6.2018-3847>.
5. Antcliff, K., Whiteside, S., Kohlman, L. W., and Silva, C., "Baseline Assumptions and Future Research Areas for Urban Air Mobility Vehicles," AIAA Scitech 2019 Forum, San Diego, CA, January 2019. DOI: <https://doi.org/10.2514/6.2019-0528>.
6. Johnson, W., "A Quiet Helicopter for Air Taxi Operations," VFS Aeromechanics for Advanced Vertical Flight Technical Meeting, San Jose, CA, January 2020.
7. Cornelius, J., "Designing a Coaxial Quadrotor for Urban Air Mobility," VFS Autonomous VTOL Technical Meeting, Mesa, Arizona, 2023.
8. Whiteside, S. K., Pollard, B. P., Antcliff, K. R., Zawodn, N. S., Fei, X., Silva, C., and Medina, G. L., "Design of a Tiltwing Concept Vehicle for Urban Air Mobility," NASA/TM- 20210017971, June 2021.
9. Johnson, W., "NASA Design and Analysis of Rotorcraft," NASA/TP - 2015-218751, April 2015.
10. Johnson, W., "NDARC — NASA Design and Analysis of Rotorcraft Validation and Demonstration," American Helicopter Society Specialists' Conference on Aeromechanics, San Francisco, CA, January 2010.
11. Johnson, W., "Rotorcraft Aeromechanics Applications of a Comprehensive Analysis," HeliJapan 1998: AHS International Meeting on Rotorcraft Technology and Disaster Relief, Gifu, Japan, April 1998.
12. Johnson, W., "Technology Drivers in the Development of CAMRAD II," American Helicopter Society Aeromechanics Specialist Meeting, San Francisco, CA, January 2018.
13. Johnson, W., "A Comprehensive Analytical Model of Rotorcraft Aerodynamics and Dynamics, Part I: Analytical Development," NASA/TM - 81182, June 1980.
14. Wachspress, D. A., Quackenbush, T. R., and Boschitsch, A., "First-Principles Free-Vortex Wake Analysis for Helicopters and Tiltrotors," American Helicopter Society 59th Annual Forum, Phoenix, AZ, May 2003.
15. Quackenbush, T., and Bliss, D., "Free Wake Calculation of Rotor Flow Fields for Interactional Aerodynamics," American Helicopter Society 44th Annual Forum, Washington DC, June 1988.
16. McVeigh, M. A., and McHugh, F. J., "Influence of Tip Shape, Chord, Blade Number, and Airfoil on Advanced Rotor Performance," 38th Annual Forum of the American Helicopter Society, Anaheim, CA, January 1982.
17. Keys, C. N., McVeigh, M. A., Dadone, L., and McHugh, F. J., "Estimation of Full-scale Rotor Performance from Model Rotor Test Data," 39th Annual Forum of the American Helicopter Society, St. Louis, MO, May 1983.

18. Hugues, P. P. D., McAlister, K. W., and Tung, C., "Effect of an Extendable Slat on the Stall Behavior of a VR-12 Airfoil," NASA T/P - 3407, September 1993.
19. Yu, Y. H., Lee, S., McAlister, K. W., and Tung, C., "Dynamic Stall Control for Advanced Rotorcraft Application," *AIAA Journal*, Vol. 33, (2), February 1995, pp. 289–295. DOI: <https://doi.org/10.2514/3.12496>.
20. Martin, P., McAlister, K., Chandrasekhara, M., and Geissler, W., "Dynamic Stall Measurements and Computations for a VR-12 Airfoil with a Variable Droop Leading Edge," 59th Annual Forum of the American Helicopter Society, Phoenix, AZ, May 2003.
21. Roedts, R. L., and Maughmer, M. D., "Rotorcraft Performance Enhancements Due to a Lower-Surface Effector," 35th European Rotorcraft Forum, Hamburg, Germany, September 2009.
22. Flemming, R., "An Experimental Evaluation of Advanced Rotorcraft Airfoils in the NASA Ames Eleven-Foot Transonic Wind Tunnel," NASA/CR - 166587, September 1984.
23. "OVERFLOW Module for AFTGen Application User Manual," Sukra Helitek, Inc.
24. Drela, M., "XFOIL: An Analysis and Design System for Low Reynolds Number Airfoils," *Low Reynolds Number Aerodynamics*, edited by T. J. Mueller, 1989. DOI: https://doi.org/10.1007/978-3-642-84010-4_1.
25. Drela, M., "A User's Guide to MSES 3.05," MIT Department of Aeronautics and Astronautics, July 2007.
26. Pulliam, T., "ARC2D - Efficient Two-Dimensional Solution Methods For The Navier-Stokes Equations," February 1994.
27. Sukra Helitek, "Rotor UNStructured Solver Application," Sukra Helitek, Inc., October 2018.
28. Nichols, R., and Buning, P. G., "User's Manual for OVERFLOW 2.3," NASA Langley Research Center, August 2010.
29. Spalart, P. R., and Allmaras, S. R., "A one-equation turbulence model for aerodynamic flows," 30th Aerospace Sciences Meeting and Exhibit, Reno, NV, January 1992. DOI: <https://doi.org/10.2514/6.1992-439>.
30. Allmaras, S. R., Johnson, F. T., and Spalart, P. R., "Modifications and Clarifications for the Implementation of the Spalart-Allmaras Turbulence Model," Seventh International Conference on Computational Fluid Dynamics, Big Island, HI, July 2012.
31. Kallstrom, K., "Exploring Airfoil Table Generation using XFOIL and OVERFLOW," VFS Aeromechanics for Advanced Vertical Flight Technical Meeting, San Jose, CA, January 2022.
32. "UIUC Airfoil Coordinates Database," University of Illinois at Urbana-Champaign.
33. Harris, C. D., "Two-Dimensional Aerodynamic Characteristics of the NACA 0012 Airfoil in the Langley 8 Foot Transonic Pressure Tunnel," NASA/TM - 81927, April 1981.
34. McCroskey, W. J., "A Critical Assessment of Wind Tunnel Results for the NACA 0012 Airfoil," NASA/TM - 100019, October 1987.
35. Smith, M. J., Wong, T.-C., Potsdam, M., Baeder, J., and Phanse, S., "Evaluation of CFD to Determine Two-Dimensional Airfoil Characteristics for Rotorcraft Applications," 60th Annual Forum of the American Helicopter Society, Baltimore, MD, June 2004.
36. Shelton, A., Abras, J., Jurenko, R., and Smith, M., "Evaluation of CFD to Determine Two-Dimensional Airfoil Characteristics for Rotorcraft Applications," 43rd AIAA Aerospace Sciences Meeting and Exhibit, Reno, NV, January 2005. DOI: <https://doi.org/10.2514/6.2005-1227>.
37. Quackenbush, T. R., Keller, J., and Whitehouse, G., "Analysis Methods for Advanced V/STOL Configurations," 72nd Annual Forum of the American Helicopter Society, West Palm Beach, FL, May 2016.
38. Quackenbush, T. R., Wachspress, D. A., and Boschitsch, A. H., "A Comprehensive Hierarchical Aeromechanics Rotorcraft Model (CHARM) for General Rotor/Surface Interaction," SBIR Phase II Technical Report 99-03, 1999.
39. Wachspress, D. A., Quackenbush, T. R., and Boschitsch, A. H., "First-Principles Free-Vortex Wake Analysis for Helicopters and Tiltrotors," 59th Annual Forum of the American Helicopter Society, Phoenix, AZ, May 2003.
40. Choi, J.-Y., Summers, M., and Corrigan, J. J., "Validation of Charm Wake Methodology for Computation of Loads and Vibrations," 65th Annual Forum of the American Helicopter Society, Grapevine, TX, May 2009.
41. Shirazi, D., "Wake Simulation of the Multirotor Test Bed and Validation of CHARM Software," NASA T/M, unpublished, 2023.
42. Quackenbush, T. R., Bliss, D. B., Wachspress, D. A., Boschitsch, A. H., and Chua, K., "Computation of Rotor Aerodynamic Loads in Forward Flight Using a Full-Span Free Wake Analysis," NASA C/R - 177611, October 1990.

APPENDIX

Appendix A

Table 5. VR-12 Legacy and OVERFLOW Δ maximum lift coefficient and Δ minimum drag coefficient.

M	$\Delta c_{l,max}$	$\Delta c_{d,min}$
0.310	0.087656	0.000730
0.355	0.074774	0.000526
0.406	0.072281	0.000339
0.454	0.124637	0.000196
0.502	0.179936	0.000084
0.550	0.191850	0.000002
0.600	0.170024	0.000044
0.650	0.272070	0.000022
0.701	0.252956	0.000209
0.750	0.132022	0.001341
0.802	0.161513	0.005187
0.824	0.079853	0.012928
0.852	0.175757	0.026441
1.000	0.156597	0.091526

Table 7. SSC-A09 Legacy and OVERFLOW Δ maximum lift coefficient and Δ minimum drag coefficient

M	$\Delta c_{l,max}$	$\Delta c_{d,min}$
0.300	0.126000	0.002441
0.307	0.118473	0.002445
0.399	0.135398	0.002499
0.400	0.135555	0.002500
0.500	0.086204	0.001697
0.599	0.048504	0.001601
0.600	0.048588	0.001601
0.603	0.049947	0.001586
0.700	0.079984	0.001100
0.703	0.088925	0.001111
0.800	0.279027	0.000835
0.804	0.301132	0.000595
0.850	0.995929	0.002162
0.920	0.844823	0.028200
0.980	0.739356	0.010500

Table 6. Average Δ between VR-12 Legacy and OVERFLOW aerodynamic coefficients.

M	Δc_l	Δc_d	Δc_m
0.000	0.1395	0.0127	0.0098
0.310	0.0466	0.0013	0.0128
0.355	0.0234	0.0013	0.0138
0.406	0.0372	0.0020	0.0142
0.454	0.0370	0.0010	0.0144
0.502	0.0776	0.0050	0.0155
0.550	0.0847	0.0095	0.0141
0.600	0.1146	0.0103	0.0173
0.650	0.1409	0.0060	0.0241
0.701	0.1297	0.0043	0.0286
0.750	0.1222	0.0061	0.0275
0.802	0.0994	0.0039	0.0274
1.000	0.1739	0.0242	0.0401

Table 8. Average Δ between SSC-A09 Legacy and OVERFLOW aerodynamic coefficients.

M	Δc_l	Δc_d	Δc_m
0.000	0.0574	0.0013	0.0136
0.300	0.0051	0.0042	0.0061
0.400	0.0360	0.0027	0.0166
0.500	0.0064	0.0088	0.0212
0.600	0.0782	0.0122	0.0174
0.700	0.0601	0.0146	0.0040
0.800	0.0434	0.0203	0.0055
0.850	0.1904	0.0922	0.0030
0.920	0.1551	0.0429	0.0058
0.980	0.0992	0.0277	0.0026

Appendix B

Additional plots for VR-12 cases are presented in Appendix B. Figure 42, 43, 44, and 45 shows the VR-12 results of C_T/σ versus collective angle for RPM 350, 400, 469, and 500.

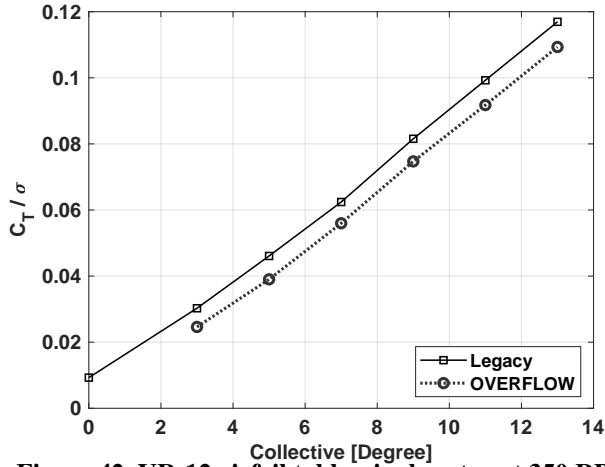


Figure 42. VR-12 airfoil table, single rotor at 350 RPM.

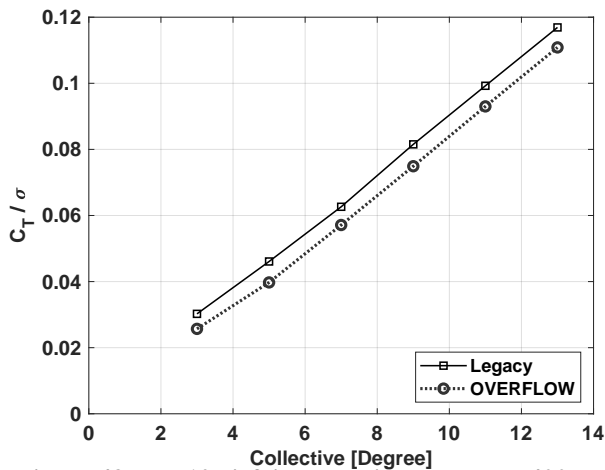


Figure 43. VR-12 airfoil table, single rotor at 400 RPM.

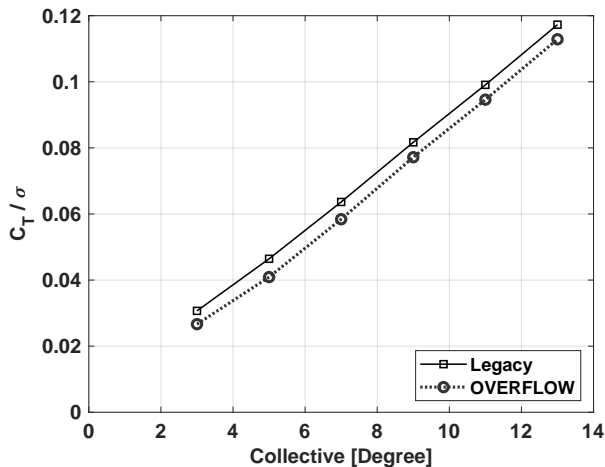


Figure 44. VR-12 airfoil table, single rotor at 469 RPM.

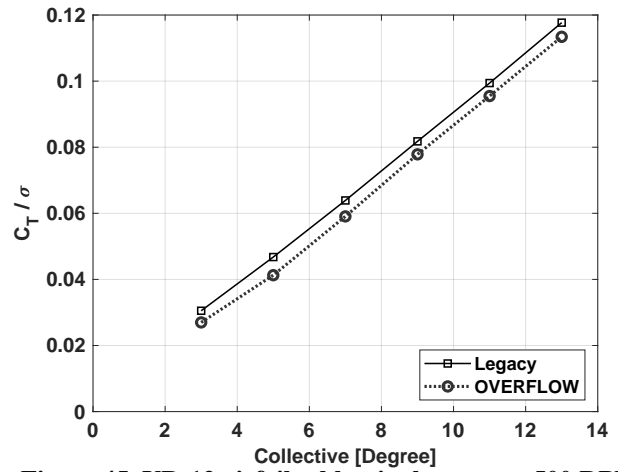


Figure 45. VR-12 airfoil table, single rotor at 500 RPM.

Figure 46, 47, 48, and 49 present the C_P/σ versus collective angle for four RPM of 350, 400, 469 and 500.

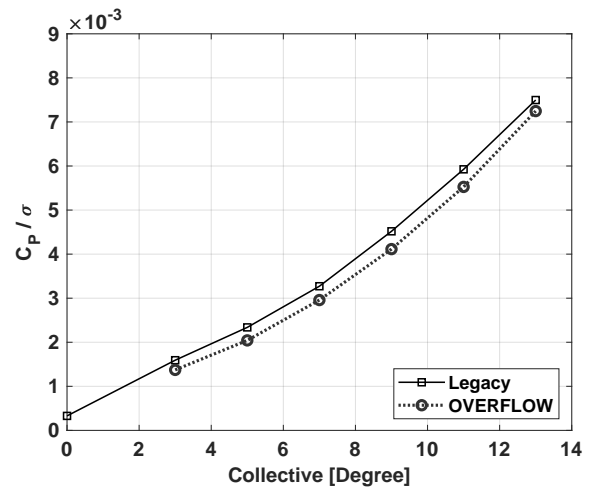


Figure 46. VR-12 airfoil table, single rotor at 350 RPM.

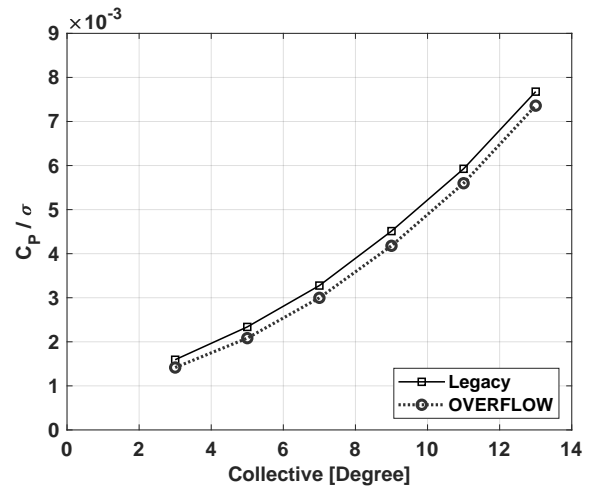


Figure 47. VR-12 airfoil table, single rotor at 400 RPM.

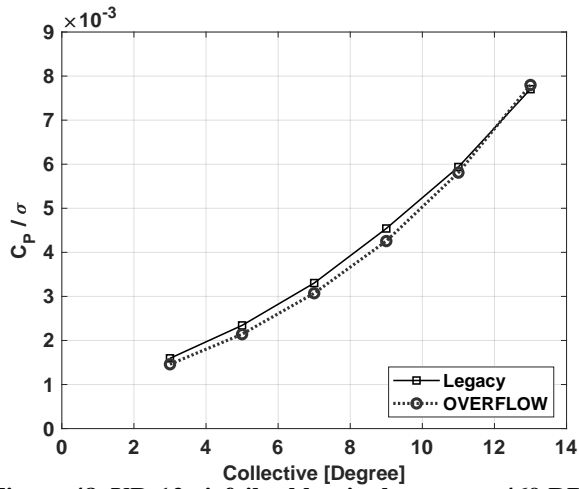


Figure 48. VR-12 airfoil table, single rotor at 469 RPM.

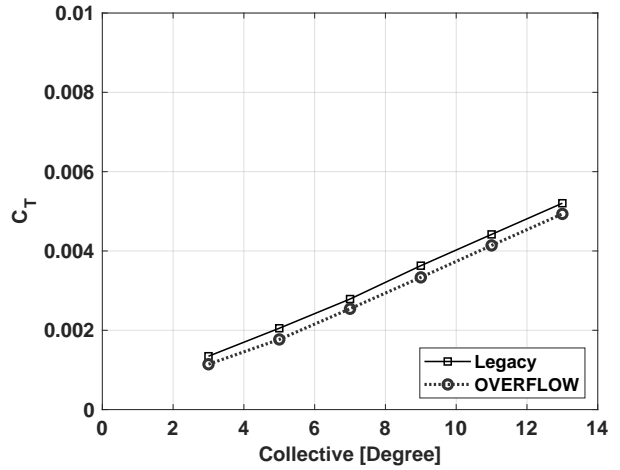


Figure 51. VR-12 airfoil table, single rotor at 400 RPM.

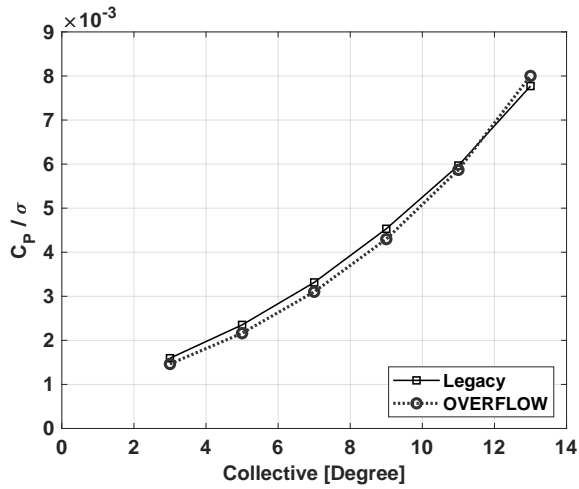


Figure 49. VR-12 airfoil table, single rotor at 500 RPM.

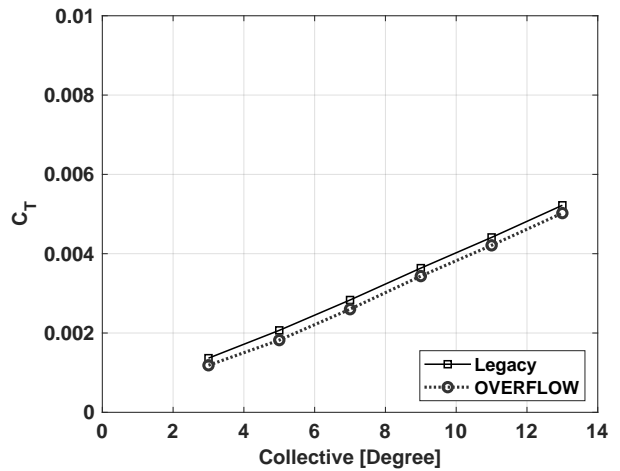


Figure 52. VR-12 airfoil table, single rotor at 469 RPM.

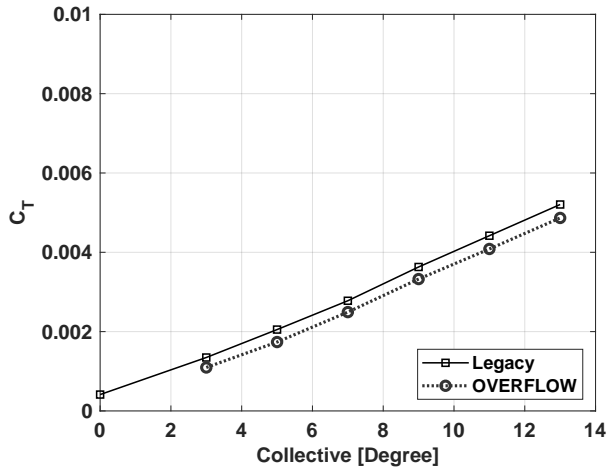


Figure 50. VR-12 airfoil table, single rotor at 350 RPM.

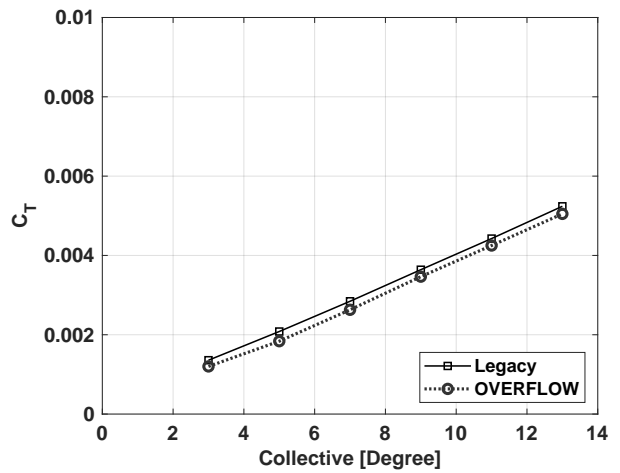


Figure 53. VR-12 airfoil table, single rotor at 500 RPM.

Appendix C

Additional plots and figures for SSC-A09 cases are presented in Appendix C. Figure 54, 55, 56, and 57 shows the C_T/σ versus collective angle.

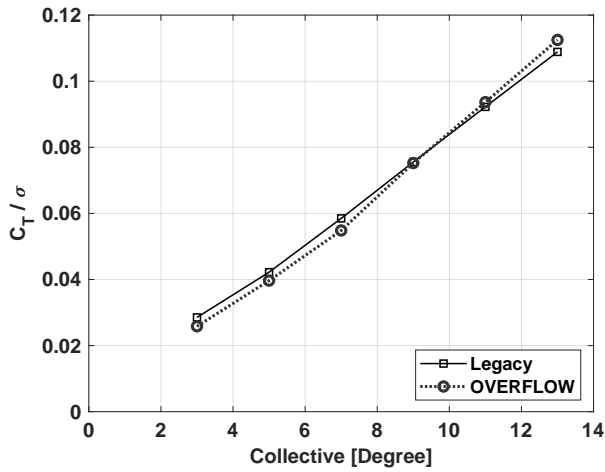


Figure 54. SSC-A09 airfoil table, single rotor at 350 RPM.

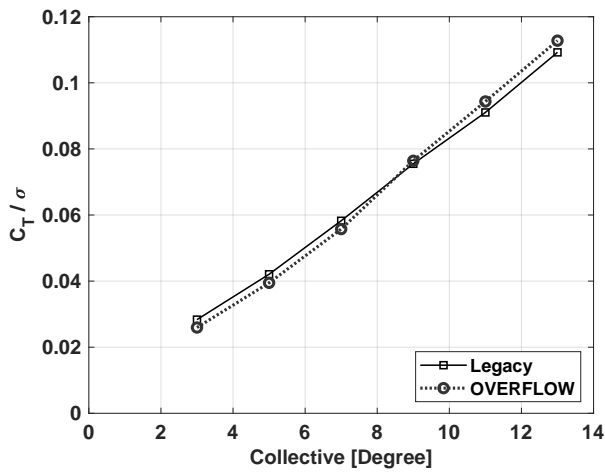


Figure 55. SSC-A09 airfoil table, single rotor at 400 RPM.

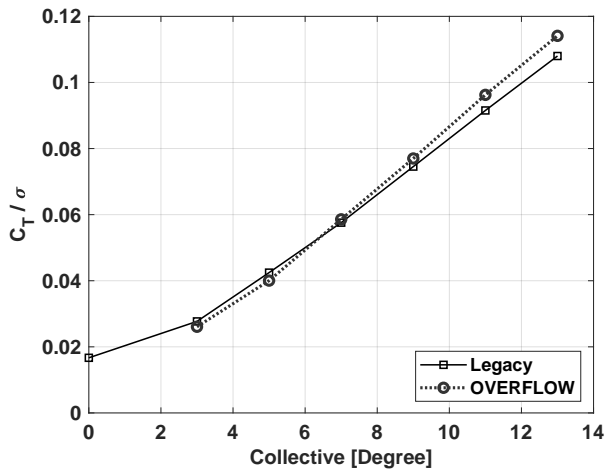


Figure 56. SSC-A09 airfoil table, single rotor at 469 RPM.

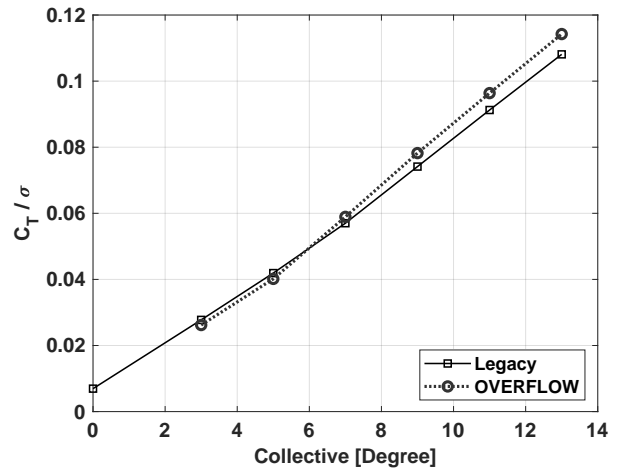


Figure 57. SSC-A09 airfoil table, single rotor at 500 RPM.

Figure 58, 59, 60, and 61 show the C_P/σ versus collective angle at four different RPM.

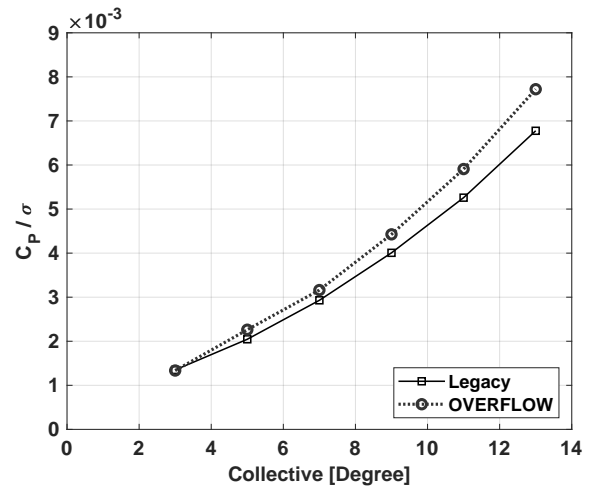


Figure 58. SSC-A09 airfoil table, single rotor at 350 RPM.

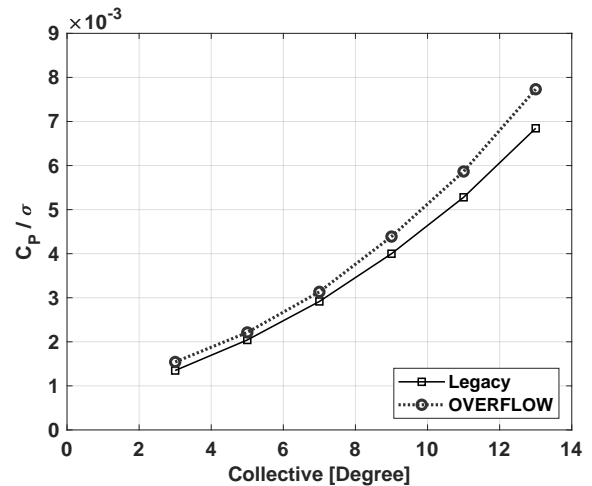


Figure 59. SSC-A09 airfoil table, single rotor at 400 RPM.

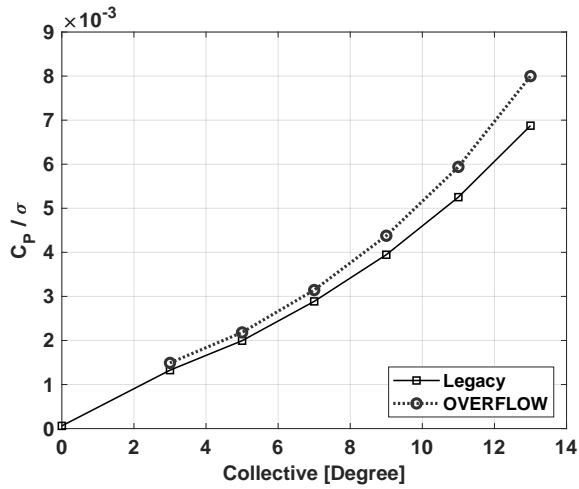


Figure 60. SSC-A09 airfoil table, r single rotor at 469 RPM.

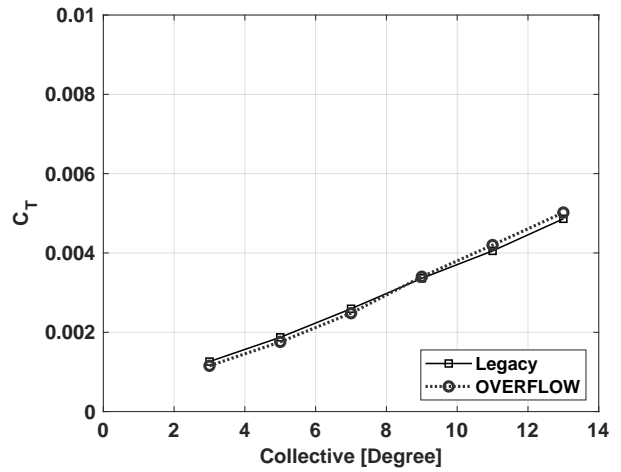


Figure 63. SSC-A09 airfoil table, single rotor at 400 RPM.

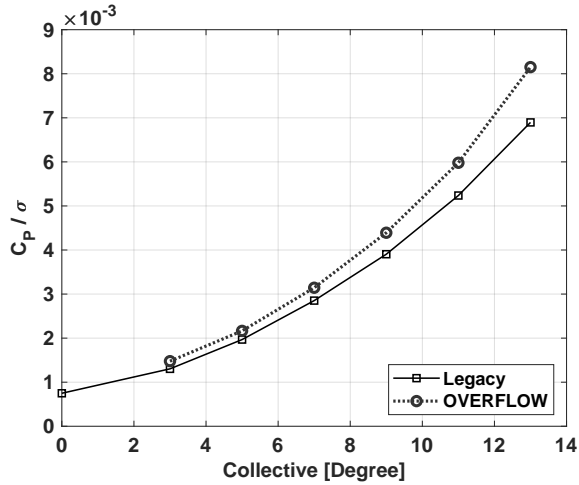


Figure 61. SSC-A09 airfoil table, single rotor at 500 RPM.

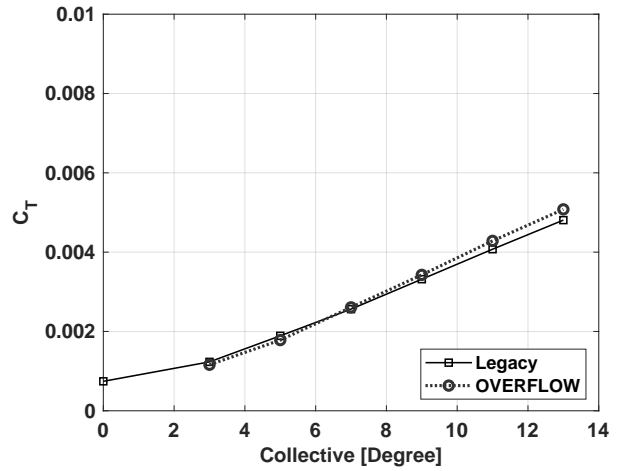


Figure 64. SSC-A09 airfoil table, single rotor at 469 RPM.

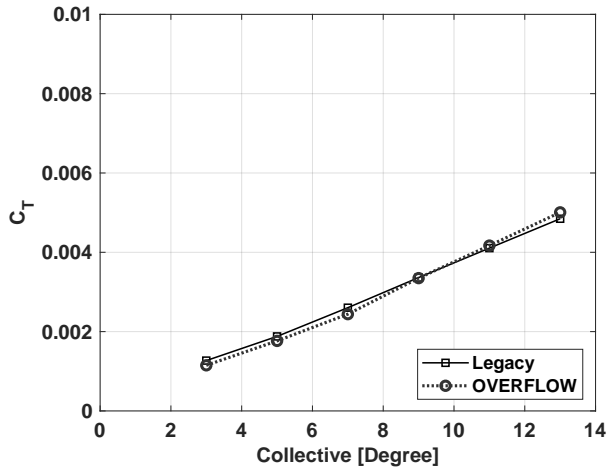


Figure 62. SSC-A09 airfoil table, single rotor at 350 RPM.

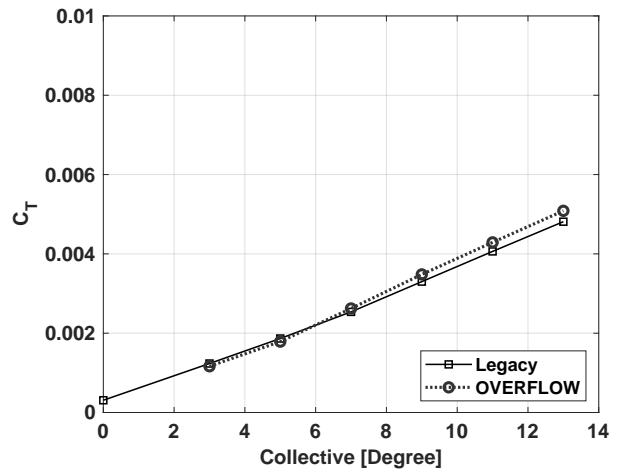


Figure 65. SSC-A09 airfoil table, single rotor at 500 RPM.

Appendix D

Additional plots and figures for the quadrotor single rotor cases are presented in Appendix D. Figure 66, 67, 68, and 69

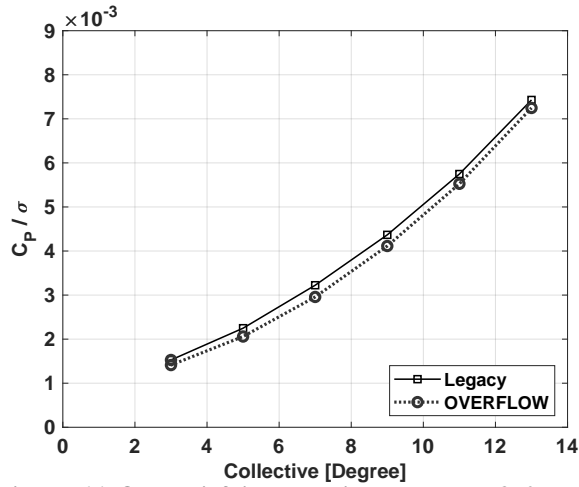


Figure 66. Quad airfoil table, single rotor at 350 RPM.

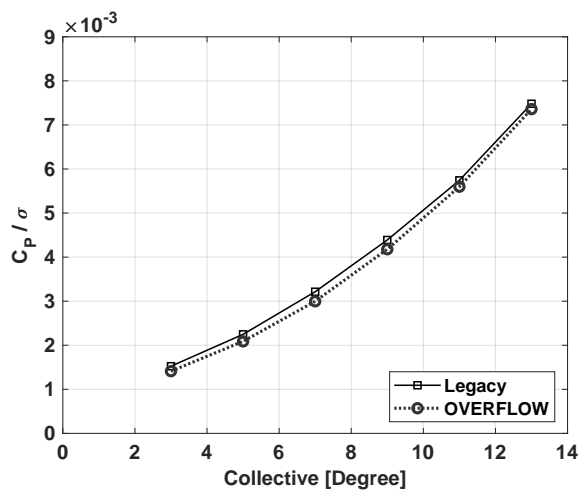


Figure 67. Quad airfoil table, single rotor at 400 RPM.

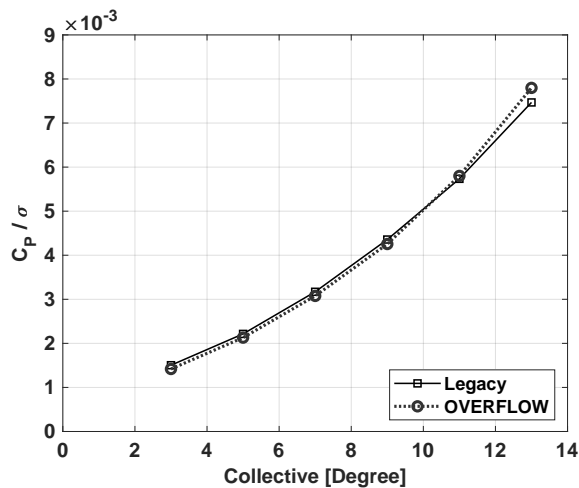


Figure 68. Quad airfoil table, single rotor at 469 RPM.

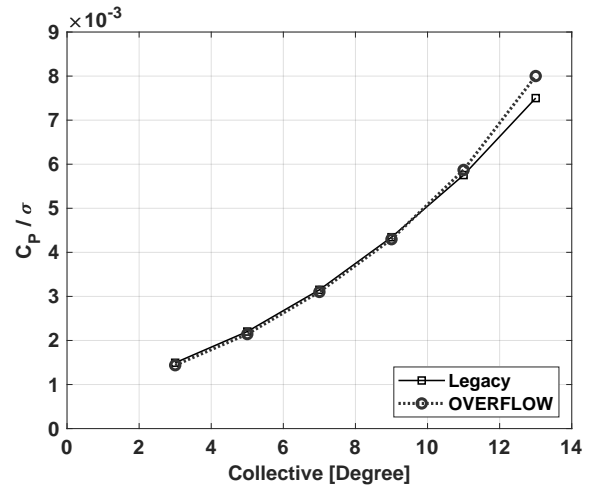


Figure 69. Quad airfoil table, single rotor at 500 RPM.

Figure 70, 70, 71, 72, and 73 show the C_T/σ versus collective angle sweep.

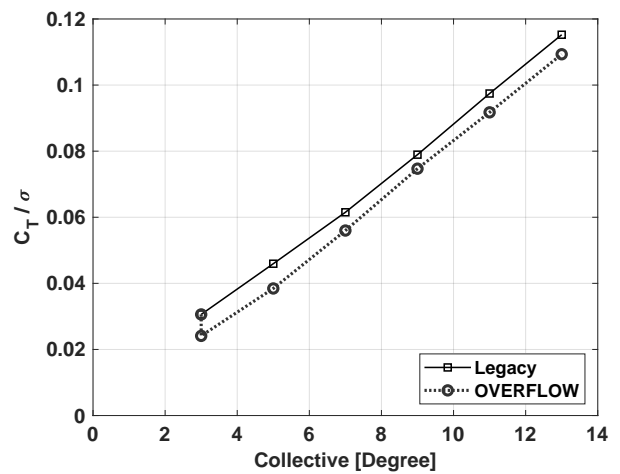


Figure 70. Quad airfoil table, single rotor at 350 RPM.

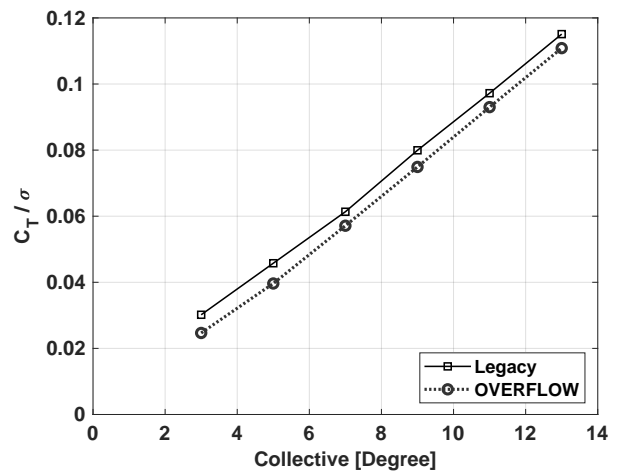


Figure 71. Quad airfoil table, single rotor at 400 RPM.

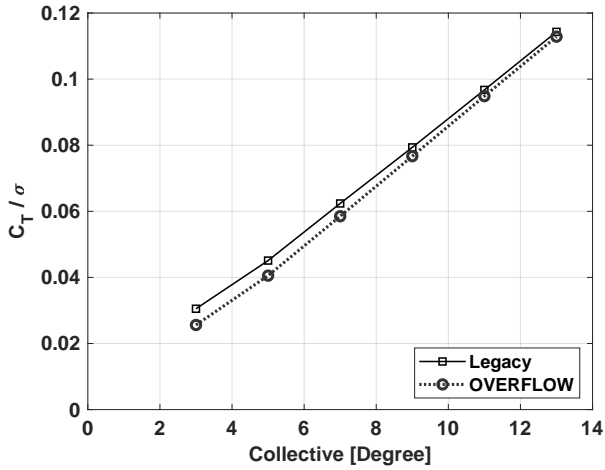


Figure 72. Quad airfoil table, single rotor at 469 RPM.

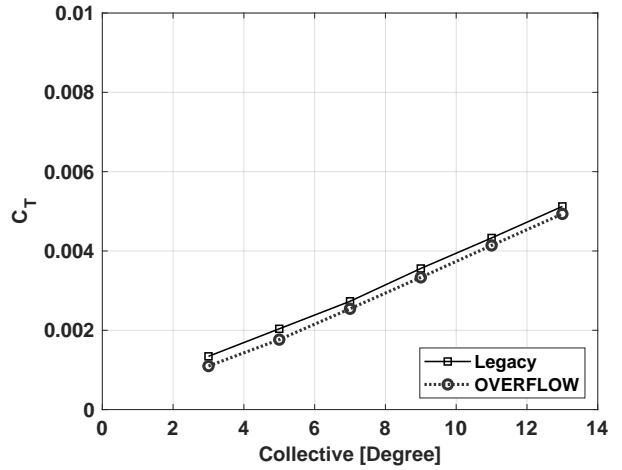


Figure 75. Quad airfoil table, single rotor at 400 RPM.

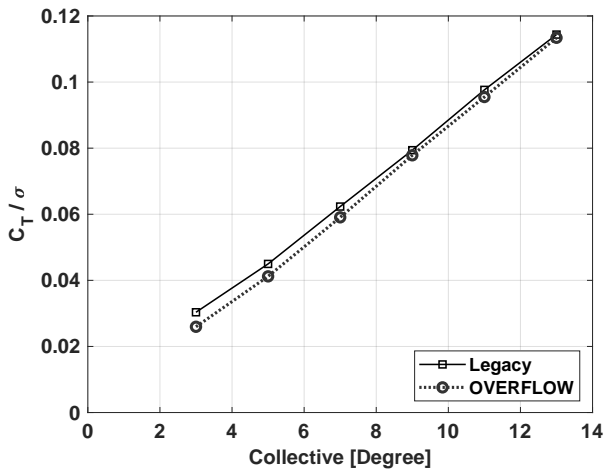


Figure 73. Quad airfoil table, single rotor at 500 RPM.

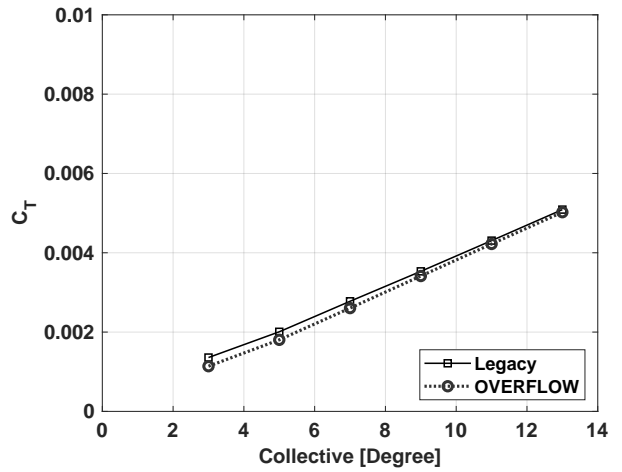


Figure 76. Quad airfoil table, single rotor at 469 RPM.

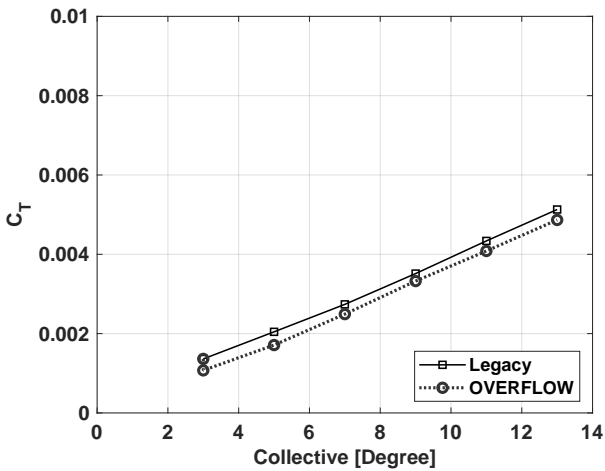


Figure 74. Quad airfoil table, single rotor at 350 RPM.

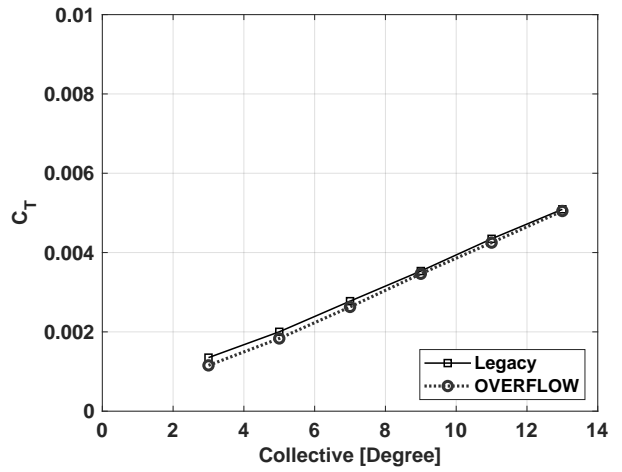


Figure 77. Quad airfoil table, single rotor at 500 RPM.